University of Southern Queensland

Faculty of Engineering & Surveying

Assisted Standing And Walking Mode For RobugIV Eight Legged Robot

A dissertation submitted by

Nils Lückemeyer

in fulfilment of the requirements of

ENG4112 Research Project

Submitted: October, 2005

Abstract

The aim of this project is to design and test an add-on spring support for the legs of Robug IV. This mechanism will allow the robot to operate with the 6bar air supply available at the University of Southern Queensland.

A model of a leg is developed and tested for its accuracy. It includes both kinematic and kinetic aspects of the leg. Loop closure equations and an iterative method are used for the kinematics. The kinetic equations are derived using the force balancing method.

The model is used to develop a good design solution for the spring mechanism and to predict its behaviour when manufactured and assembled.

University of Southern Queensland

Faculty of Engineering and Surveying

ENG4111/2 *Research Project*

Limitations of Use

Certification of Dissertation

I certify that the ideas, designs and experimental work, results, analyses and conclusions set out in this dissertation are entirely my own effort, except where otherwise indicated and acknowledged.
I further certify that the work is original and has not been previously submitted for assessment in any other course or institution, except where specifically stated.

Nils Lückemeyer

0050035042

Signature

Date

Acknowledgments

While working on this project I received support from a number of people. I would like to thank the McDonald family for all their help and for making my year in Australia the experience it was. I would also like to thank my German family and Federica Pelzer for all their moral support they gave me although they were so far away. I would like to thank the German Academic Exchange service for making my studies in Australia possible by granting me a scholarship. I would like to thank my supervisors Chris Snook and Prof. John Billingsley for their guidance.

Nils Lückemeyer

University of Southern Queensland

October 2005

Contents

Abstract i

Acknowledgments iv

List of Figures x

List of Tables xv

Chapter 1 Introduction 1

1.1 Project outline 1

1.2 Dissertation overview 1

Chapter 2 Legged Robots 3

2.1 Overview 3

2.2 Mobile robotics 3

2.3 Reasons for legged robotics 4

2.4 Brief history of walking robots 5

2.5 Current projects 7

2.5.1 The Honda walking robots 7

2.5.2 Adaptive suspension vehicle 8

2.5.3 Silex 9

2.5.4 MECANT and WorkPartner 10

2.6 Summary 12

Chapter 3 The Robug Projects **13**

3.1 Chapter Overview 13

3.2 Robug I 14

3.3 Robug II 14

3.4 Robug III 15

3.5 Robug IV 16

3.5.1 Robug IV at the University of Southern Queensland 17

3.6 Summary 17

Chapter 4 Modelling a Leg **18**

4.1 Overview 18

4.2 Requirements and Assumptions 18

4.3 Kinematics 21

4.3.1 Definition of variables and constants 21

4.3.2 Dimensions 21

4.3.3 Equations 23

4.3.4 Starting values 24

4.4 Springs 25

4.5 Kinetics 28

4.5.1 Forces 28

4.5.2 Cylinder pressures 31

4.6 Weight of the leg 32

4.7 Summary 33

Chapter 5 Model Validation **34**

5.1 Overview 34

5.2 Test arrangement 34

5.3 Modifications of the model 35

5.4 Comparison of model and experiment 37

5.5 Summary 45

Chapter 6 Design of the mechanism **46**

6.1 Overview 46

6.2 Overall Optimisation 46

6.3 Limited range of motion approach 47

6.3.1 Typical range of motion 47

6.3.2 Types of motion 48

6.3.3 Selection of a position 48

6.4 Summary 52

Chapter 7 Manufacture and Assembly of the exoskeletal system 53

7.1 Chapter Overview 53

7.2 Necessary parts 53

7.3 Production and assembly 55

7.4 Summary 56

Chapter 8 Further analysis of the final mechanism 57

8.1 Overview 57

8.2 Estimated pressures 58

8.2.1 Typical range of motion 58

8.2.2 Whole range of motion 59

8.3 Stability 63

8.3.1 Typical range of motion 65

8.3.2 Whole range of motion 67

8.4 Dead points 67

8.5 Summary 67

Chapter 9 Conclusions and Further Work 68

9.1 Achievement of Project Objectives 68

9.2 Further Work 69

9.2.1 Test and quantification of the final system 69

9.2.2 Other modes of operation 70

References **71**

Appendix A Project Specification **74**

Appendix B Source Code **76**

B.1 Introduction 77

B.2 Starting values 77

B.3 Model 78

B.4 Model Validation 82

B.4.1 Modified model 82

B.4.2 Comparison of model and test 85

B.5 Mechanism design 86

B.6 Pressure plots 88

B.6.1 Typical range of motion 88

B.6.2 Whole range of motion 89

B.7 Stability 89

List of Figures

2.1 Merlin holding a pipe bomb 4

2.2 Rygg's mechanical horse 6

2.3 evolution of Honda's two-legged robots 8

2.4 The Adaptive Suspension Vehicle demonstration its towing capability . 9

2.5 Silex, the walking robot developed by the Free University of Brussels. . 10

2.6 MECANT walking in the type of environment it was designed for. . . . 11

2.7 WorkPartner 11

3.1 Robug I with creator Arthur Collie 13

3.2 Robug II 14

3.3 Robug III 15

3.4 Robug IV 16

4.1 degrees of freedom, side and top view 19

4.2 applied forces, side and top view 20

4.3 definition of angles and lengths 22

4.4 effect of a good and bad set of starting values 24

4.5 characteristics of the first spring 26

4.6 characteristics of the second spring 27

4.7 free body diagram 29

4.8 upper cylinder piston free body diagram 31

4.9 lower cylinder piston free body diagram 31

5.1 test arrangement 35

5.2 comparison of test and model for $r_3 = 0.291$m and the springs located in position 1 37

5.3 comparison of test and model for $r_3 = 0.287$m and the springs located in position 3 38

5.4 comparison of test and model for $r_3 = 0.287$m and the springs located in position 5 39

5.5 comparison of test and model for $r_3 = 0.336$m and the springs located in position 1 40

5.6 comparison of test and model for $r_3 = 0.336$m and the springs located in position 3 41

5.7 comparison of test and model for $r_3 = 0.336$m and the springs located in position 5 42

5.8 comparison of test and model for $r_3 = 0.381$m and the springs located in position 1 43

5.9 comparison of test and model for $r_3 = 0.381$m and the springs located in position 4 44

5.10 comparison of test and model for $r_3 = 0.381$m and the springs located in position 5 45

6.1 plot of the absolute value of $maxp$ for $-0.030\text{m} \leq n \leq 0.070\text{m}$ and $0.020\text{m} \leq h \leq 0.110\text{m}$. 49

6.2 plot of the absolute value of $maxp$ using the association shown in equation 6.4. 50

6.3 plot of the minimum and maximum spring force depending on the spring position. 51

6.4 position with the largest spring force value 52

6.5 position with the smallest spring force value 52

7.1 technical drawing of the first plate 54

7.2 technical drawing of the second plate 54

7.3 spring mechanism 55

8.1 pressures in cylinders r_7 (black) and r_3 (gray) when standing up for the typical range of motion, $n = 0.001$m and $h = 0.060$m. The horizontal lines indicate ± 5bar. 58

8.2 pressures in cylinders r_7 (black) and r_3 (gray) when standing for the typical range of motion, $n = 0.001$m and $h = 0.060$m. The horizontal lines indicate ± 5bar. 59

8.3 pressures in cylinders r_7 (black) and r_3 (gray) when lifting a leg for the typical range of motion, $n = 0.001$m and $h = 0.060$m. The horizontal lines indicate ± 5bar. 59

8.4 pressure in cylinder r_7 when standing up. $n = 0.001$m and $h = 0.060$m. 60

8.5 pressure in cylinder r_3 when standing up. $n = 0.001$m and $h = 0.060$m. 60

8.6 pressure in cylinder r_7 when standing. $n = 0.001$m and $h = 0.060$m. . . 61

8.7 pressure in cylinder r_3 when standing. $n = 0.001$m and $h = 0.060$m. . . 61

8.8 pressure in cylinder r_7 when lifting a leg off the ground. $n = 0.001$m and $h = 0.060$m. 62

8.9 pressure in cylinder r_3 when lifting a leg off the ground. $n = 0.001$m and $h = 0.060$m. 62

8.10 schematic drawing of a two-way cylinder 63

8.11 difference between a stable position and an unstable one 64

8.12 stability of cylinder r_7 (black) and cylinder r_3 (grey) when standing up . 65

8.13 stability of cylinder r_7 (black) and cylinder r_3 (grey) when standing . . 66

8.14 stability of cylinder r_7 (black) and cylinder r_3 (grey) when lifting a leg off the ground 66

8.15 4 bar linkage 67

A.1 Project Specification 75

B.1 source code to calculate the starting values 78

B.2 model source code page 1 79

B.3 model source code page 2 80

B.4 model source code page 3 81

B.5 modified model source code page 1 83

B.6 modified model source code page 2 84

B.7 modified model source code page 3 85

B.8 comparison of model and test source code 86

B.9 maximum pressure source code 87

B.10 source code used to plot the pressures for the typical range of motion . . 88

B.11 source code used to plot the pressures for the whole range of motion . . 89

B.12 source code used to examine the stability of a position within the typical range of motion 90

List of Tables

4.1 coordinates to describe the displacement of a leg 19

4.2 measured dimensions 21

4.3 starting values 24

4.4 weight on and length of the first spring 25

4.5 weight on and length of the second spring 26

4.6 weight distribution 33

5.1 spring positions on the plate used in the test arrangement 35

5.2 modified weight distribution 36

5.3 lower cylinder fixed at $r_3 = 0.291$m, spring located in position $k = 1$ . . 37

5.4 lower cylinder fixed at $r_3 = 0.287$m, spring located in position $k = 3$ . . 38

5.5 lower cylinder fixed at $r_3 = 0.287$m, spring located in position $k = 5$ . . 39

5.6 lower cylinder fixed at $r_3 = 0.336$m, spring located in position $k = 1$ . . 40

5.7 lower cylinder fixed at $r_3 = 0.336$m, spring located in position $k = 3$ . . 41

5.8 lower cylinder fixed at $r_3 = 0.336$m, spring located in position $k = 5$ . . 42

5.9 lower cylinder fixed at $r_3 = 0.381$m, spring located in position $k = 1$ . . 43

5.10 lower cylinder fixed at $r_3 = 0.381$m, spring located in position $k = 4$ . . 44

5.11 lower cylinder fixed at $r_3 = 0.381$m, spring located in position $k = 4$ . . 45

B.1 nomenclature 77

B.2 Nomenclature for the model. Protected expressions can only be seen within the model they are used in. 82

B.3 Additional nomenclature for the comparison plots. 85

B.4 Additional nomenclature for the max. pressure source code. 87

Chapter 1

Introduction

1.1 Project outline

Legged robotics have a long history. One of the newer projects is Robug IV, an eight legged robot powered by air pressure. It was not originally built at the University of Southern Queensland, nor did the laboratory at the University of Southern Queensland possess a compressor with a high enough pressure to operate the robot.

The aim of this project is to design, model and test an add-on spring support for the legs of Robug IV so that it can be operated on the 6bar available at the USQ laboratory.

1.2 Dissertation overview

Chapter 2 gives an introduction to the history of legged robotics and a number of legged robots.

Chapter 3 deals with the four different Robug projects and their history.

Chapter 4 describes the development of a model that is used for the design of the spring mechanism.

Chapter 5 deals with the test arrangement used to test the model and compares its result to the one of the model.

Chapter 6 describes how the add-on spring mechanism is designed.

Chapter 7 deals with the manufacture and assembly of the exoskeletal system.

Chapter 8 gives a prediction for the behaviour of the new exoskeletal system.

Chapter 9 contains final conclusions and states what further works need to be done.

Chapter 2

Legged Robots

2.1 Overview

The main focus in this chapter is the history of walking robots. The first two sections give a short introduction to what legged robots are and why they are of such interest. A number of projects will be introduced to illustrate the technological development.

2.2 Mobile robotics

Legged robots is one category of mobile robotics. A mobile robot can be defined as a machine that is able to move from one location to another without human interaction. Mobile robots can be air-based, water-based or land-based.

Most of the world's robots are not mobile. They are automated stationary machines that use manipulatory arms for one specific purpose such as welding. This type of robot can be widely found in industrial production.

Stationary robots work in a known environment. Mobile robots need to be able to handle complex and changing environments. This makes the design of mobile robots much more complex. A very high level of artificial intelligence is required for the control system and the mechanics need to be strong enough to withstand uncontrollable factors.

The benefits of mobile robots are clear – they are flexible, as they can change location and this opens up a whole new field of applications to robotics. Transportation and work in hazardous areas are two of such applications.

‘Legged’ implies that the robot is land-based. Three types of land-based mobile robots exist: legged, wheeled and tracked. Wheeled and tracked robots are easier to develop as the number of degrees of freedom is much smaller. However, legged robotics have the widest application range.

One example of a tracked robot is Merlin. Because it can be remotely controlled, it is used to defuse bombs. This way humans can stay at a safe distance from the bomb.

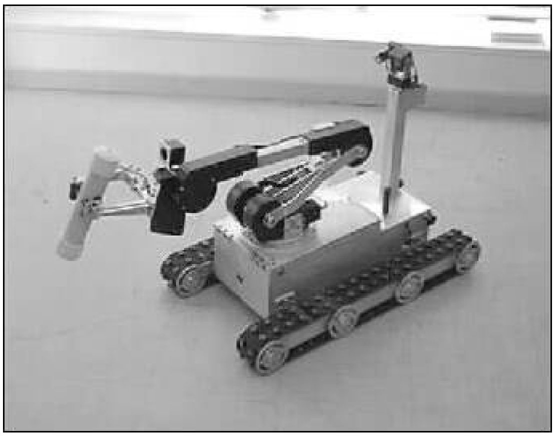

Figure 2.1: Merlin holding a pipe bomb

Although tracked robots can operate on a larger range of surfaces than wheeled robots, they do not have the flexibility humans or animals have. This explains the need for legged robots.

2.3 Reasons for legged robotics

Using legs can be seen as the most natural way of motion on land. Humans and animals use legs to walk and can access most terrains. A typical example that indicates the limitations of wheeled locomotion is stairs. For vehicles such as cars or wheelchairs, stairs are an insurmountable obstacle. They can only be used on especially prepared surfaces such as roads.

Humans, in contrast, can access rough terrains – forests, mountains or stairs. With legs obstacles such rocks or fallen trees can be avoided. If legged robotics succeed this can be seen as a revolution of locomotion. Machines would be able to access all terrains that humans can access and possibly more. For example they could be able to climb walls like spiders.

The Chernobyl nuclear catastrophe indicated the necessity for legged robotics. Hazardous areas usually have a rough terrain that cannot be accessed by wheeled machines. Humans on the other hand would put themselves at a massive medical risk in such a catastrophe. Legged robots could be used to clear hazardous places without the risk of injury or death. Such applications could be the handling of dangerous chemical or radioactive materials.

2.4 Brief history of walking robots

It is difficult to date back the beginnings of legged robotics. Lewis (2002) sees the beginning of research into walking machines in the 1960's when the Phoney Pony was built at the University of Southern California. *Milestones in the Development of Legged Robots* (1999) on the other hand indicates that the first milestone in the development of legged robots was in 1836 when Weber and Weber showed that the natural frequency of a leg when swinging as a compound pendulum is similar to the cadence in live walking.

These differences in perspective occured as some sources only list legged robotics projects that were planned or completed while other sources also recognise preliminary research that did not pursue the aim of actually building a walking robot.

In 1872 the Governor of California, Leland Stanford, asked Eadweard James Muybridge to help settle a $25,000 bet (Miller & Hemsath 2004). Muybridge was to prove whether or not horses have all four feet in the air simultaneously at some point when running. It took him five years to develop the necessary techniques to stop motion photography and in 1977 Muybridge could prove that a horse indeed lifts all four feet at some point while running. After this success he continued photographing animals in motion documenting their gaits and published *The horse in motion* in 1877.

In 1893 L. A. Rygg obtained a patent for his design called "The Mechanical Horse" (Witte 2000). It looks like a crossing between a horse and a bicycle. A person would sit on the back of the horse and use pedals to power it. There is no evidence that the design was ever successfully built.

Figure 2.2: Rygg's mechanical horse

In 1913 a patent was granted to Bechtolsheim for another human-powered machine (Galt 1998). The design was radically different than Rygg's design. Although probably more realistic, no evidence of successfully building the 4-legged machine exists.

Although the idea of walking machines already existed at the end of the 18th century, technology had not progressed enough until about 1960 to actually build walking machines. Considered to be the first computer controlled is the Phoney Pony, built in the 1960's at the University of Southern California (Lewis 2002). The aspect of computer control gave walking machines a new dimension. This was the start of turning legged machines into legged robots.

Probably the first commercially used walking machine was Big Muskie. The Big Muskie was a giant dragline owned by the Central Ohio Coal Company (Malkamaki 2004). Construction began in 1966 and in 1969 Big Muskie was ready to remove overburden from coal formations. It weighed 13,500 tons, had a bucket capacity of 325 tons and was powered by 13,800 volts. Hydraulically driven feet were used to walk. Big Muskie was used until 1991 when it was no longer needed due to a depression in the demand for Ohio coal.

In 1977 the OSU Hexapod was presented at the Ohio State University (Galt 1998). The six-legged robot weighed 150kg and its legs were built to emulate insect legs. Continual improvements made the USO Hexapod one of the most successful legged robot research projects.

All of the legged robots mentioned above had at least 4 legs that allowed a statically stable motion. This means that the robot could stand in a statically balanced position on a number of legs while one or more legs were moved to the next position. Marc Raibert developed a one-legged robot at the Carnegie-Mellon University in 1983 (Galt 1998). With only one leg, static equilibrium is impossible. The static equilibrium needs to be replaced by a dynamic one. This is similar to riding a bicycle which is stable as long as it is driven at a certain speeds but falls to one side when it comes to stop. Achieving a dynamic equilibrium is difficult as a complex and very accurate control system using sensors and micro-processors is needed. Raibert's machine was able to hop in one place, travel, keep its balance when disturbed and jump over small obstacles.

When finishing the Adaptive Suspension Vehicle project, Song & Waldron (1988) published the much recognised book *Machines that walk* in which they discuss gait analysis, gaits for level walking and for irregular terrain, coordination, leg and ankle design. According to Galt (1998) this book was the first that provided in-depth treatment of statically stable walking machines and might be the most cited work used by legged robotics researchers.

2.5 Current projects

2.5.1 The Honda walking robots

Honda started research and development of two-legged humanoid robots in 1986 (Honda 2005). Until today 11 experimental models, prototypes and humanoid robots were built. The first experimental model in 1986 was used to examine the principles of two legged locomotion. Within the next four experimental models E1 to E4 Honda was able to switch from static to dynamic locomotion and increased the walking speed from 0.25km/h to 4.7km/h. The last two experimental models E5 and E6 were used to implement autonomous control.

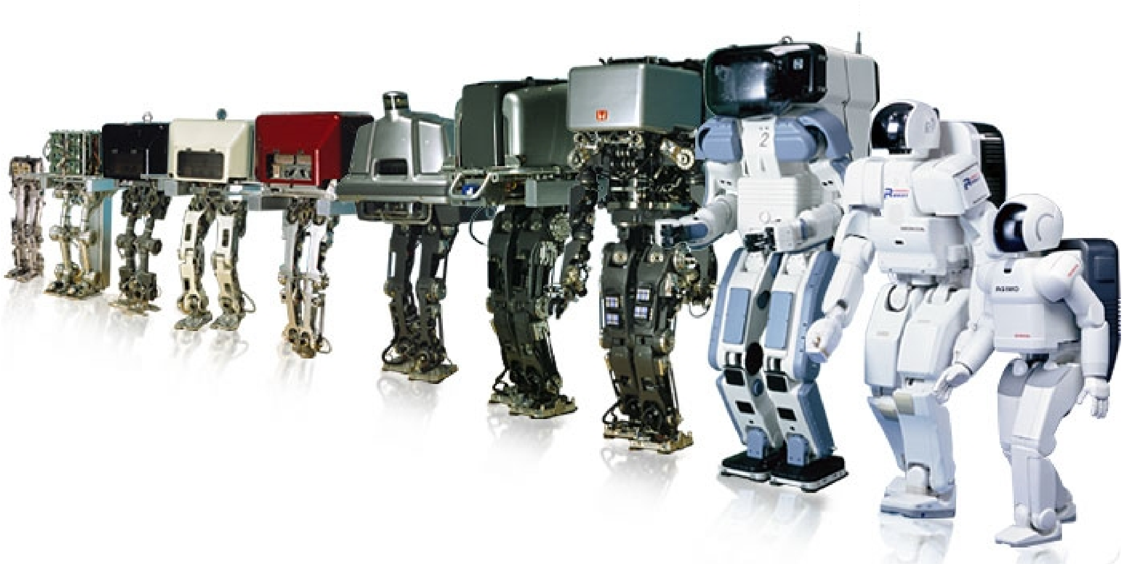

Figure 2.3: evolution of Honda's two-legged robots

Between 1993 and 1997 Honda built 3 prototypes of humanoid two-legged robots. The second one, P2, was the world's first self regulated two-legged humanoid robot. It was 1.82m tall and weighed 210kg. P2 was able to walk independently, walk up and down stairs, push carts and perform other operations. It has astounded researchers with its performance (Galt 1998).

In the year 2000 Honda presented Asimo that has a further advanced walking technology. In comparison with P2 both height and weight were drastically reduced to 1.2m and 43kg (Honda 2001).

2.5.2 Adaptive suspension vehicle

The above mentioned adaptive suspension vehicle is one of the larger legged robots with approximate dimensions 5x3x2m and a weight of 3200kg (Galt 1998). A four cylinder petrol engine was used to power the legs.

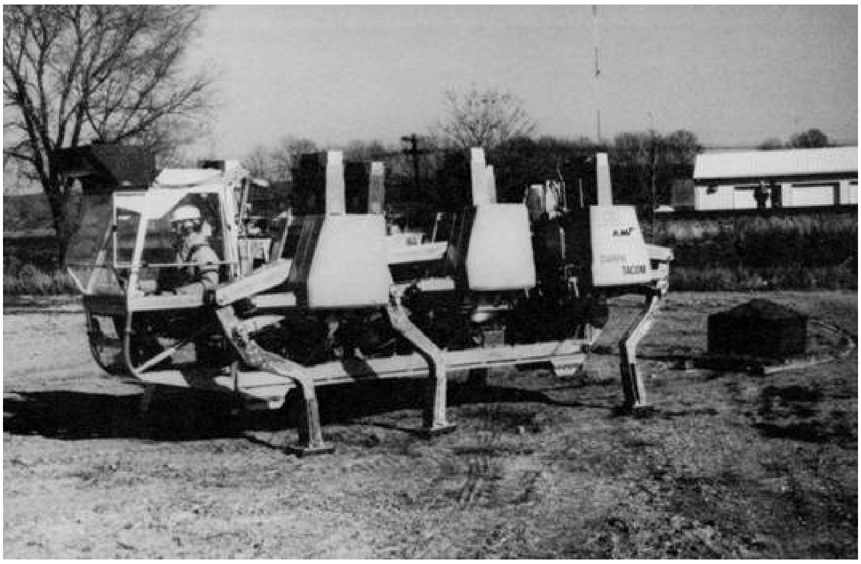

Figure 2.4: The Adaptive Suspension Vehicle demonstration its towing capability

The ASV project started in 1982 and finished in 1990. Before Honda presented its humanoid prototypes the ASV was the most sophisticated, self-contained and practical walking machine ever developed.

2.5.3 Silex

Silex is a 6-legged robot developed by the Active Structure Laboratory (ASL) at the Free University of Brussels. It weighs 13kg and is 50cm high (ASL 2005). Each leg has three degrees of freedom that are controlled by DC motors.

The interesting part about Silex is its decentralised structure: each leg is controlled by its own INTEL 87C196KC microcontroller. Three different levels of control were implemented. The lowest level handles the leg trajectory and force control and is implemented at the leg level in the 6 microcontrollers. The next highest level includes gait and height control, the force distribution at the robot level and is automated. The highest level is dealing with planning of direction and speed. These can be controlled by a user with a joystick.

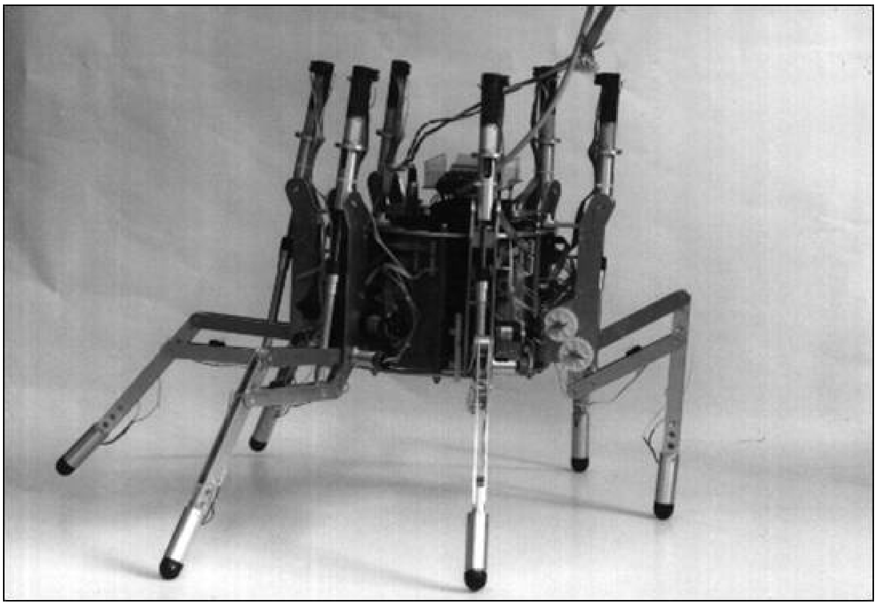

Figure 2.5: Silex, the walking robot developed by the Free University of Brussels.

2.5.4 MECANT and WorkPartner

Mecant was developed by the Automation Technology Laboratory at the Helsinki University of Technology in Finland. It is a fully independent hydraulic six-legged walking machine that weighs about 1100kg (*MECANT, the Walking Machine* 2005). The hydraulic system used to operate the legs is powered by a 38 kW 2-cylinder ultra-light aeroplane engine with air cooling. The leg mechanism is a 2-dimensional pantograph that can rotate around the vertical axis. The control system consists of a computer network connecting seven on-board computers , sensors for the vehicle body and legs, and a portable operator interface with radio control and communication facilities. The vehicle is controlled remotely by an operator.

The MECANT project has been highly successful and its design has been used to develop a legged tree cutter (Galt 1998). The success of MECANT is based on the motion control system that is capable of terrain adaptation.

By now the MECANT project has been finshed und is succeeded by WorkPartner, a light weight service robot. WorkPartner works interactively with people and is designed to carry out everyday tasks in outdoor environments (*WorkPartner - Information* 2005). Two manipulator arms allow the robot to execute tasks.

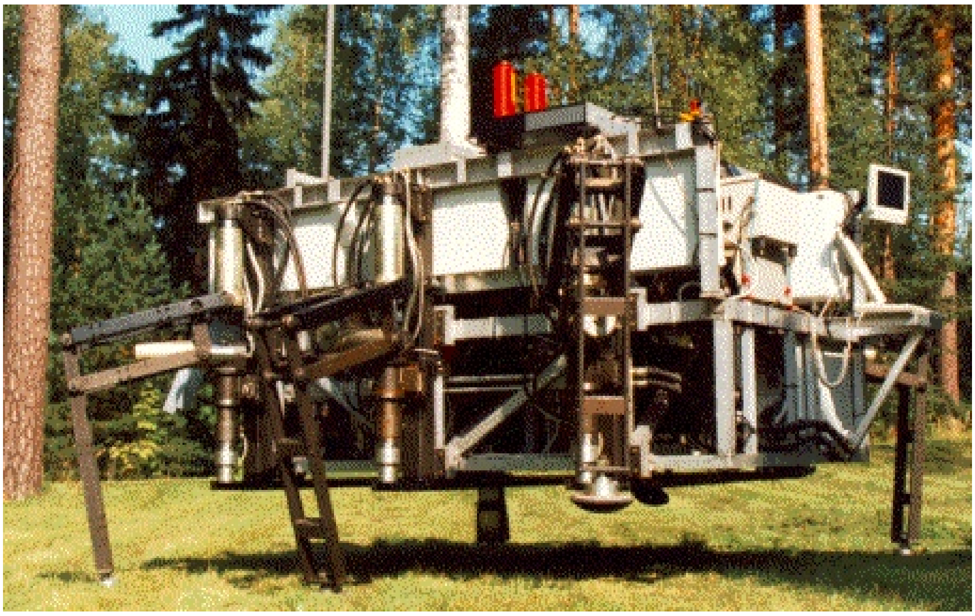

Figure 2.6: MECANT walking in the type of environment it was designed for.

A very interesting concept is the use of a hybrid locomotion system. It allows motion with legs and/or wheels at the same time. Such a system is more complex than a normal wheeled or legged robot, but there is an opportunity to combine the benefits of both legged and wheeled robots.

Figure 2.7: WorkPartner

2.6 Summary

Legged robots are one category of mobile robots. The first research on the gait of animals can be dated back more than 100 years. At the end of the 19th century the first ideas for walking machines existed, but it was not until the 1960's that a number of research groups succeeded in building legged robots. Some legged robots such as Big Muskie were commercially used, but most of them were research projects that were trying to develop the necessary mechanics and control systems.

Chapter 3

The Robug Projects

3.1 Chapter Overview

Robug IV, which is currently located at the University of Southern Queensland, was not a single project, but one in a large series of projects. The Robug projects were developed by the Mobile Robotics Group (MRG) at the University of Portsmouth and Portech. This chapter gives an introduction to the 4 Robugs.

Figure 3.1: Robug I with creator Arthur Collie

3.2 Robug I

The very first walking robot developed by the MRG, Robug I, was a six-legged walking robot base powered by compressed air (Galt 1998). It is displayed in figure 3.1 with the robot's chief design engineer Professor Arthur Collie.

3.3 Robug II

Robug II was primarily not a walking but a climbing robot. Apart from its own 12kg weight it can carry another approximately 12kg up a vertical wall (*Staunen, was die Zukunft bringt* 2003). When it climbs, Robug II first tests whether the necessary adhesion exists between the moving leg and the wall before the next leg is moved.

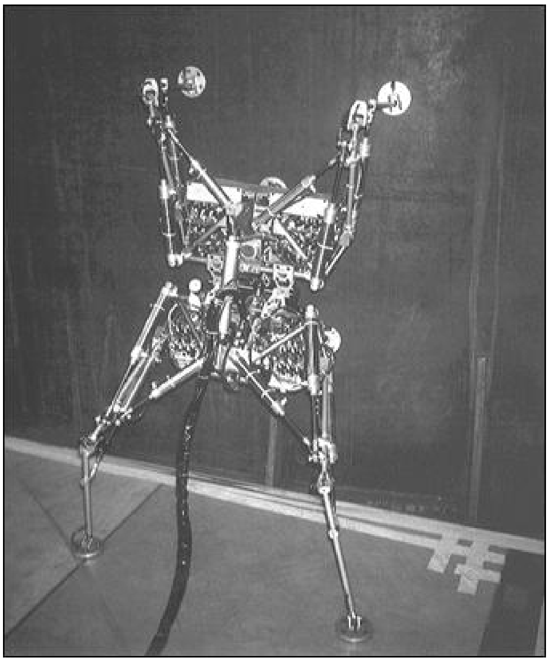

Figure 3.2: Robug II

The robot has 4 legs, each powered by 3 pneumatic cylinders (Galt 1998). The legs each had three degrees of freedom and were organised as a spider-like structure. The body was split into two modules that were joined by a pivot with a pneumatic cylinder to bend the body. This mechanical configuration allowed Robug II to become the first known robot to be able to transfer autonomously from the floor to a vertical wall.

Like Silex Robug II has one microcontroller per leg. They were programmed with rule-based behaviours to provide the robot with advanced capabilities such as searching for footholds.

3.4 Robug III

Robug III was inspired by spiders and crabs (*Robug III* 2000). Its body is 0.8m long, 0.6m wide and 0.6m high and has eight 1m long pneumatically powered legs. Although being a walking robot it can climb walls like Robug II with its vacuum gripper feet. Four joints in each leg allow the robot to navigate over uneven terrain with a maximum speed of 6m per minute.

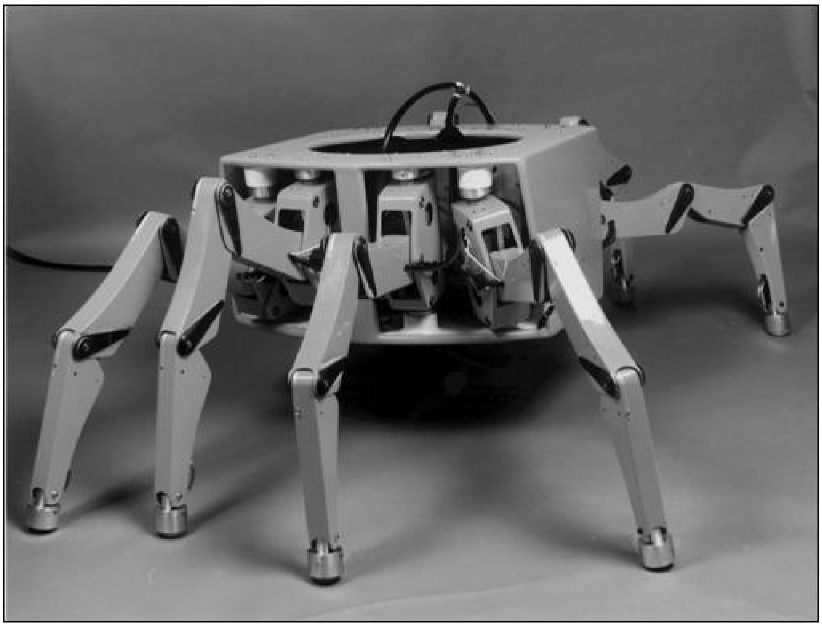

Figure 3.3: Robug III

The cylinders are driven by a pneumatic drive system at 1300kPa (Galt 1998). These high pressures are used to achieve a high power-to-weight ratio which allows higher payload capabilities while minimising the possibility of damage when operating in unstructured environments.

Robug III uses two different walking strategies (Galt 1998). 'Crab walking' is used to move sideways through narrow passages. Apart from this, the Robug is capable of a longitudinal, spider-like gait. Robug III exhibited many significant advances in legged robot research, in particular the demonstrated power-to-weight ratio and climbing abilities.

3.5 Robug IV

The latest Robug project is Robug IV. Like Robug III it is an eight-legged pneumatically actuated robot. It is capable of autonomous omnidirectional walking and climbing and supports highly modular Plug-N-Play features (Waterman, Hewer & Cooke n.d.).

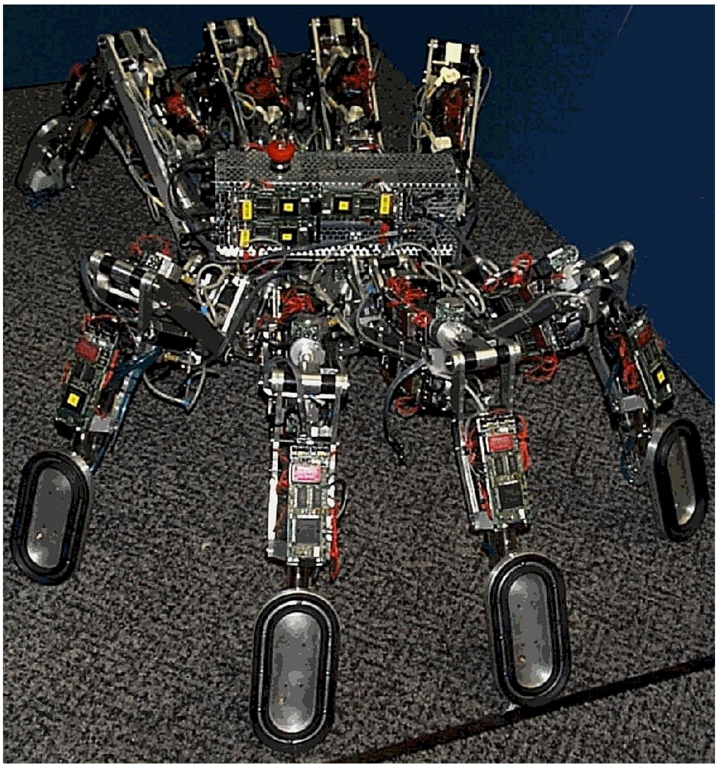

Figure 3.4: Robug IV

The design is 'spider-like'. Attached to a central body are eight legs. Each leg is 0.7m long and has four actuated joints. Vacuum gripper feet allow the Robug to climb vertical walls. The abductor, hip, and knee joints operate at up to 14bar, and the ankle joint at 8bar in order to achieve a high power-to-weight ratio.

The control of the robot is highly distributed. Thirty-two embedded controllers are used, one for each joint in each leg. After a long study Infineons (formerly Siemens) 20 MHz, 16-bit C167CR microprocessor was chosen. The CAN (Control Area Network) standard was selected as an ideal method of providing communications between different processors distributed on the robot. This standard is used in other harsh environments such as under bonnets in the automotive industry and has been well proven.

3.5.1 Robug IV at the University of Southern Queensland

Robug IV was acquired by the Faculty of Engineering and Surveying at the University of Southern Queensland. It is now dissassembled in the Advanced Control laboratory. The vacuum gripper feet were replaced by rubber feet and the ankle joints were eliminated so that each leg now only has three degrees of freedom.

At this stage it is not possible to operate Robug IV at the University of Southern Queensland due to missing control software and the air compressor at the Advanced Control Laboratory delivers only 6 bar and not the 14bar Robug IV was originally designed for. This is the reason for this project – the power-to-weight ratio is too small without any supporting mechanism.

3.6 Summary

Robug IV, which is currently located at the University of Southern Queensland, was the latest out of four Robug projects. At this stage it is not possible to operate Robug IV.

Chapter 4

Modelling a Leg

4.1 Overview

The legs of RobugIV already exist. The weight of the robot is to be supported by a new add-on spring mechanism. A prototype of this mechanism exists, but it needs to be optimised. This chapter deals with creating a model for one leg of Robug IV in order to optimise the spring mechanism. Firstly the requirements and expectations of the model will be stated and then the kinematics and kinetics of a leg will be discussed. A complete source code of the model written in MATHEMATICA can be found in appendix B.

4.2 Requirements and Assumptions

A model should always be as detailed as necessary and as simple as possible. Details are necessary to achieve the required precision, but a very complex model is difficult to create and its computation takes a lot of time. The first step in creating a model of Robug IV is to state its requirements:

- **Number of modelled legs**

  All eight legs of RobugIV are equivalent. For that reason only a model of one leg needs to be made. In later work this model could be used to create a further model of the whole robot, but this is not necessary in order to support the weight of the robot.

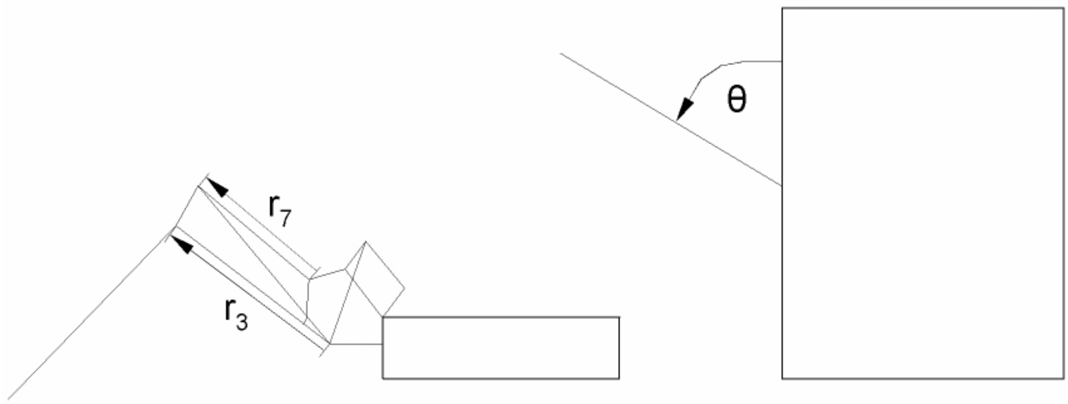

Figure 4.1: degrees of freedom, side and top view

- **Degrees of freedom**

  There are three cylinders for each leg, and therefore each leg has three degrees of freedom as can be seen in figure 4.1. One cylinder moves the lower part of the leg, and one the upper. A third cylinder in the torso rotates the whole leg. The displacement or position of the leg can be described by three coordinates, one for each cylinder. These are defined in table 4.1

Table 4.1: coordinates to describe the displacement of a leg

coordinate	description
r_3	length of the lower cylinder in the leg
r_7	length of the upper cylinder in the leg
θ	angle between leg and torso

- **Applied forces**

  Forces on the rubber foot can be applied in any direction, as shown in figure 4.2. They create forces within the leg and on the hip joints. However the component F_θ does not effect the cylinders inside the leg and the spring mechanism. On a smooth surface both horizontal force components equal 0.

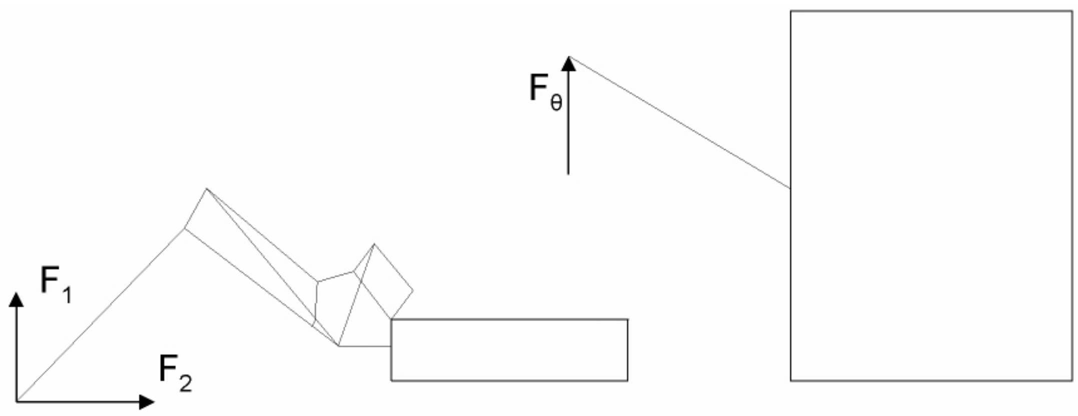

Figure 4.2: applied forces, side and top view

- **Model dimension**

  Both cylinders inside the leg and the spring mechanism are in one plane. Neither the angle θ nor the force component F_θ affects them. Hence there is no need to make a three dimensional model. A two dimensional model can include all the aspects that are important to the spring mechanism.

- **Gravity**

  Gravity is a crucial factor. Without gravity there would be no need to design a mechanism to support the leg. However, the effects of gravity on a complex system like the RobugIV leg are difficult to model. The first model neglects the weight of the leg and only considers the weight of the torso. As shown in chapter 5, this model does not explain the test results.

  In order to achieve better results, a second model includes the effects of gravity with some simplifications. It concentrates the mass in three points. Doing so leads to results which are a lot more accurate.

- **Inertia**

  A model could include dynamic effects or neglect them. Force equals mass times acceleration. Assuming that the legs move only slowly, acceleration is close to 0 and the inertial forces are therefore negligible.

- **Friction**

  Friction exists in every joint of the leg. Both models assume this friction to be negligible. This assumption is valid for well lubricated smooth joints.

- **Input and output**

  In order to optimise the spring mechanism and limit the pressure in the cylinders, the model needs to calculate the pressures in the cylinders. That is the output. The pressures depend on the lengths of the cylinders, the mounting position of the spring on the plates and the forces on the foot. These are the input variables. Thus the model can be seen as a function for the pressures, depending on a number of variables.

4.3 Kinematics

4.3.1 Definition of variables and constants

The leg can be described as a linkage made up of a number of bars and joints, a plate and, of course, the springs. In order to describe the leg mathematically, a number of variables and constants is defined. These can be found in figure 4.3. All the lengths except for r_3 and r_7 are constant, while all the angles except for ϕ_1 and ϕ_6 are variable.

4.3.2 Dimensions

Drawings of the different parts of the legs were not available, so the only way to get the dimensions of the leg was to measure them. Although this might not be the most accurate way, it has the advantage that mistakes that other people have made are not propagated. The measured dimensions can be found in table 4.2. The range of motion

Table 4.2: measured dimensions

r_1	0.104m	r_2	0.334m	r_4	.098m
r_5	0.057m	r_6	0.066m	r_9	.397m
a_3	0.057m	a_8	0.074m	b_3	.007m
ϕ_1	$\frac{22}{180}\pi$	ϕ_6	1.867		

for the cylinders is $0.225\text{m} \leq r_7 \leq 0.280\text{m}$ and $0.285\text{m} \leq r_3 \leq 0.380\text{m}$.

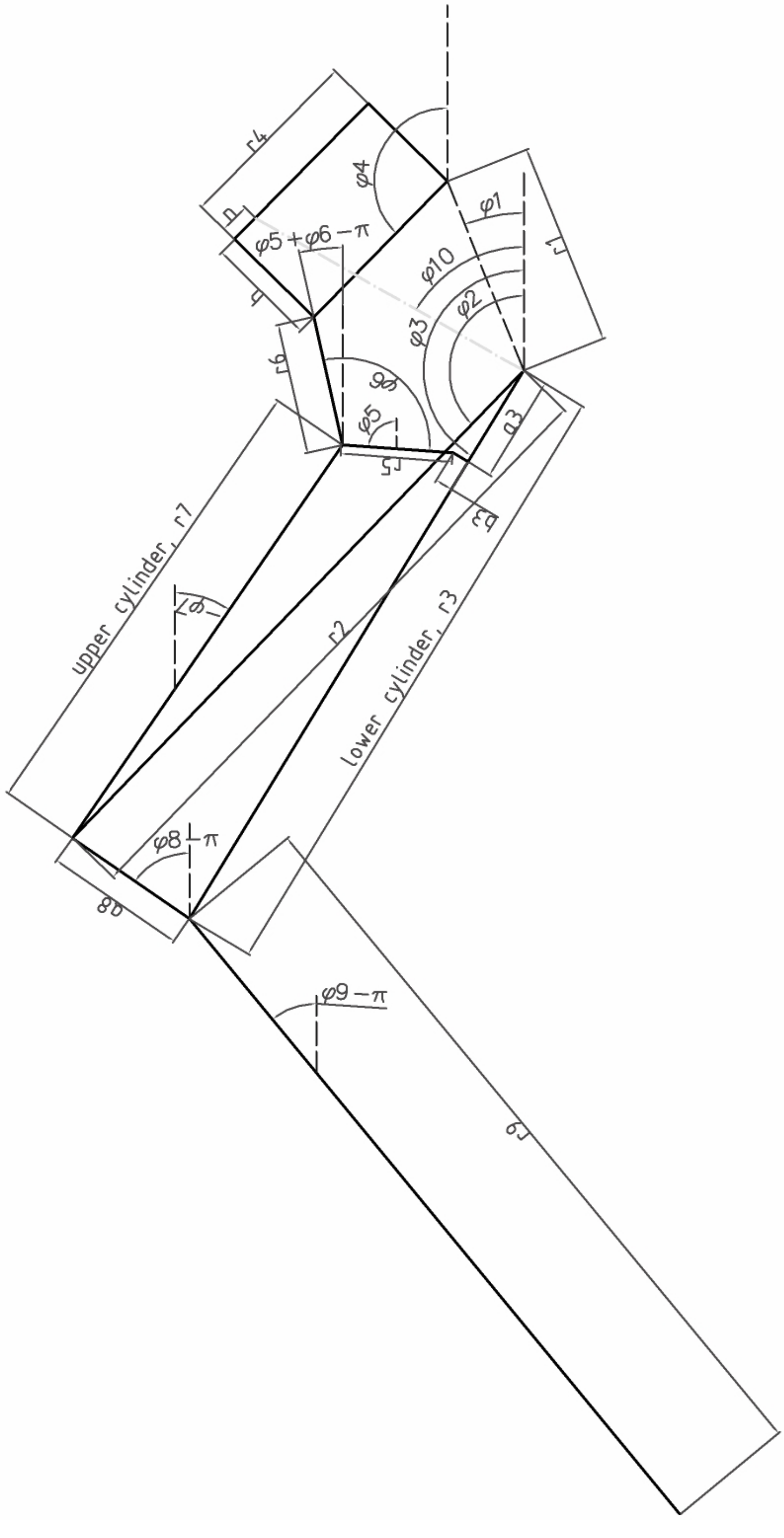

Figure 4.3: definition of angles and lengths

4.3.3 Equations

The kinematic problem could be solved analytically or numerically. Because of the high number of non-linear equations it is more reasonable to choose an iterative method. One method to derive the necessary equations is using 'loop closure equations' (Mabie & Reinholtz 1987*a*).

For each position of the cylinders six unknown angles exist: ϕ_2, ϕ_3, ϕ_4, ϕ_5, ϕ_7 and ϕ_8. ϕ_9 and ϕ_{10} are not necessary to describe the position of the leg, so they can be calculated later. The following equations can be derived:

$$\begin{aligned}
r_1 \sin\phi_1 + r_4 \sin\phi_4 - r_6 \sin(\phi_5 + \phi_6 - \pi) & \\
- r_5 \sin\phi_5 - b_3 \sin(\phi_3 - 0.5\pi) - a_3 \sin\phi_3 &= 0 \quad (4.1)\\
r_1 \cos\phi_1 + r_4 \cos\phi_4 - r_6 \cos(\phi_5 + \phi_6 - \pi) & \\
- r_5 \cos\phi_5 - b_3 \cos(\phi_3 - 0.5\pi) - a_3 \cos\phi_3 &= 0 \quad (4.2)\\
r_5 \sin\phi_5 - r_7 \sin\phi_7 + a_8 \sin\phi_8 - (r_3 - a_3)\sin\phi_3 + b_3 \sin(\phi_3 - 0.5\pi) &= 0 \quad (4.3)\\
r_5 \cos\phi_5 - r_7 \cos\phi_7 + a_8 \cos\phi_8 - (r_3 - a_3)\cos\phi_3 + b_3 \cos(\phi_3 - 0.5\pi) &= 0 \quad (4.4)\\
r_2 \sin\phi_2 + a_8 \sin\phi_8 - r_3 \sin\phi_3 &= 0 \quad (4.5)\\
r_2 \cos\phi_2 + a_8 \cos\phi_8 - r_3 \cos\phi_3 &= 0 \quad (4.6)
\end{aligned}$$

A very efficient method to solve these equations numerically is the multi-variable Newton Method. A benefit of Mathematica is, that it has a function called *FindRoot* built in that solves equations using Newton methods (Wolfram Research 2005*a*). After using this method, ϕ_9 can be calculated according to equation 4.7, where $\frac{16}{180}\pi$ is a measured value.

$$\phi_9 = \phi_8 - \frac{16}{180}\pi \tag{4.7}$$

ϕ_{10} is given by the equation:

$$\phi_{10} = \arctan\left(\frac{r_1 \sin\phi_1 + (r_4 - n)\sin\phi_4 - h\cos\phi_4}{r_1 \cos\phi_1 + (r_4 - n)\cos\phi_4 + h\sin\phi_4}\right) \tag{4.8}$$

The signs of both numerator and denominator are very important to determine ϕ_{10} in the correct quadrant, as the tangent function is π-periodic. Mathematica provides a function that automatically takes care of the quadrants.

4.3.4 Starting values

The Newton Method needs a starting value for every unknown. Different starting values can lead to different results, if the set of equations has more than one solution. This is the case for the leg as can be seen in figure 4.4. The left solution is correct, the right solution solves the equation, but is physically impossible. Hence it is important to choose a good set of starting values to obtain the correct results.

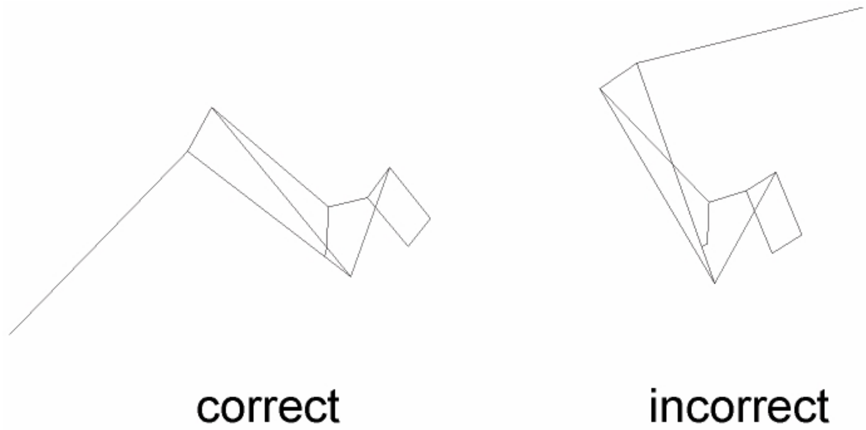

Figure 4.4: effect of a good and bad set of starting values

Another effect of good starting values is that they accelerate the calculation by decreasing the number of computations necessary to achieve a certain level of accuracy.

Table 4.3: starting values

variable	starting value for	value [rad]
$start_2$	ϕ_2	2.545
$start_3$	ϕ_3	2.767
$start_4$	ϕ_4	2.490
$start_5$	ϕ_5	1.491
$start_7$	ϕ_7	-0.4224
$start_8$	ϕ_8	4.247

It is highly desirable to have one set of starting values that works for the whole range of motion. One idea is to use the results of the angles that positioned the cylinders somewhere in the middle of their range of motion. Doing this for $r_3 = 0.3325$m and $r_7 = 0.2525$m leads to the results shown in table 4.3. The source code can be found in appendix B. A test reveals that these values lead to the correct results for the complete range of motion.

4.4 Springs

For every spring exists a characteristic relation between its length l and the applied force F. In the easiest case this relation is linear and the spring can mathematically be represented by the linear equation

$$F = k \cdot (l - l_0) \tag{4.9}$$

where k is the spring coefficient and l_0 the theoretical unstretched length of the spring. l_0 is not necessarily the length that the spring returns to when no external force is applied, because in some cases the coils of the spring touch each other so that the spring cannot return to the unstressed state and therefore remains longer than l_0.

Each leg of the Robug uses two springs of the same kind. I did a series of measurements to find out whether this linear model is valid for the Robug's springs and to find values for k and l_0

Table 4.4: weight on and length of the first spring

weight [kg]	length [m]
0.0	0.1050
0.8	0.1051
1.2	0.1051
1.5	0.1055
1.8	0.1063
2.2	0.10735
2.7	0.1090
3.2	0.1106
3.9	0.1128

I attached weights to the springs. The weights stretched the spring due to gravity and

I measured both the mass of the weights and the length of the spring. The data can be found in tables 4.4 and 4.5.

Table 4.5: weight on and length of the second spring

weight [kg]	length [m]
0.0	0.1065
0.8	0.1065
1.2	0.1068
1.5	0.1068
1.8	0.1071
2.2	0.1081
2.7	0.1096
3.2	0.1112
3.9	0.1134

Analysis of this data leads to the result that a certain threshold force is needed before the length of the spring changes. Once the length changes, the change is linear to the applied force as shown in figures 4.5 and 4.6. The lines represent the mathematical model. They can be found by using the methods of linear regression for that section, where the length of the spring changes.

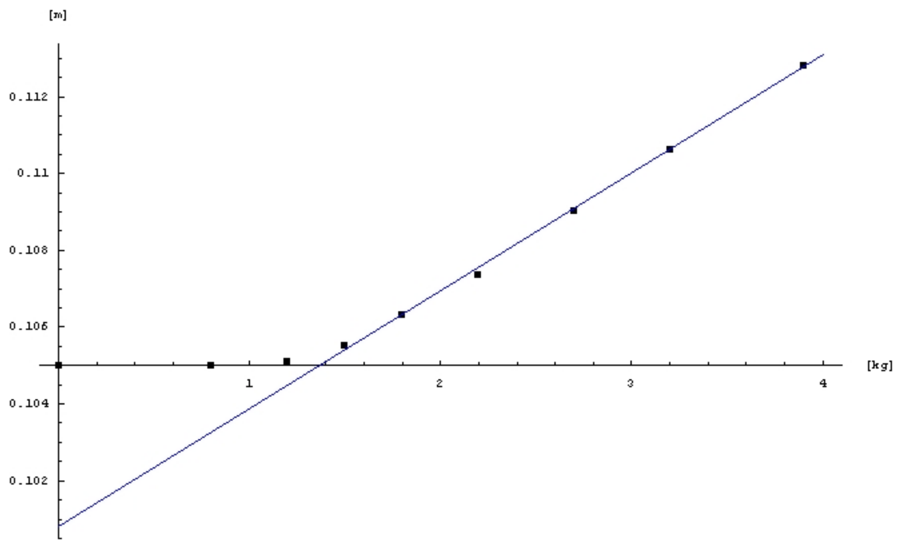

Figure 4.5: characteristics of the first spring

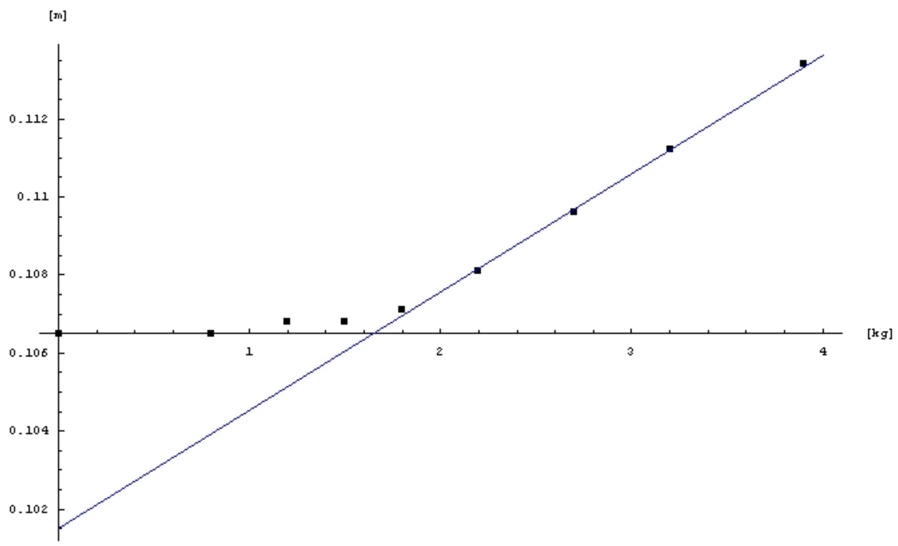

Figure 4.6: characteristics of the second spring

The unstressed length of spring 1 is then $l_{01} = 0.1008\text{m}$ and the unstretched length of spring 2 is $l_{02} = 0.1015\text{m}$. The respective spring coefficients are $k_1 = 3195\text{N/m}$ and $k_2 = 3239\text{N/m}$.

$$F = F_1 + F_2 \tag{4.10}$$

as the two springs are in parallel. Equations 4.9 and 4.10 can be combined to calculate the overall k:

$$k = k_1 + k_2 = 6434\text{N/m} \tag{4.11}$$

and the overall l_0:

$$l_0 = \frac{l_{01} \cdot k_1 + l_{02} \cdot k_2}{k_1 + k_2} = 0.10115\text{m} \tag{4.12}$$

Knowing the spring parameters, only the length r_{10} of the springs is necessary to calculate the spring force F_{18}. r_{10} can be calculated as:

$$\begin{aligned} r_{10} \quad = \quad & 0.00875\text{m} + \Big((r_1 \sin\phi_1 + (r_4 - n)\sin\phi_4 - h\cos\phi_4)^2 \\ & + (r_1 \cos\phi_1 + (r_4 - n)\cos\phi_4 + h\sin\phi_4)^2 \Big)^{-2} \end{aligned} \tag{4.13}$$

During the experiments the springs were measured from one end to the other. The 0.00875m is a correction term, as the springs sit on the bolt on one side. The bolt radius is 5mm and the coil diameter of the spring is 2.5mm. On the other side the springs go through the middle of the bolt, so only half the coil diameter is added. That makes $5 + 2.5 + 1.25 = 8.75$mm.

Now the spring force can be calculated:

$$F_{18} = k \cdot (r_{10} - l_0) \tag{4.14}$$

4.5 Kinetics

4.5.1 Forces

One way to derive the necessary equations is the force-balancing method. It requires the free body diagrams of all parts of the leg. Cylinders can be modelled as bars with a variable length. These free body diagrams are shown in figure 4.7.

Equations for body (1):

$$F_1 + F_4 + F_5 = G_1 + G_4 \tag{4.15}$$

$$F_2 + F_3 + F_6 = 0 \tag{4.16}$$

$$\begin{aligned} -F_1 r_9 \cos(\phi_9 - \pi) + F_2 r_9 \sin(\phi_9 - \pi) \\ + G_1 l_{G1} \cos(\phi_9 - \pi) - F_5 a_8 \cos(-\phi_8) \\ - F_6 a_8 \sin(-\phi_8) &= G_1 (l_{G1} \cos\phi_9 \\ &\quad + h_{G1} \cos(\phi_9 - 0.5\pi)) \end{aligned} \tag{4.17}$$

Equations for body (2):

$$-F_{10} + F_{14} + F_{13} = 0 \tag{4.18}$$

$$-F_{11} + F_{15} + F_{12} = 0 \tag{4.19}$$

$$\begin{aligned} F_{14} r_5 \cos(\pi - \phi_5) + F_{15} r_5 \sin(\pi - \phi_5) \\ + F_{13} r_6 \cos(\phi_5 - \pi + \phi_6) - F_{12} r_6 \sin(\phi_5 - \pi + \phi_6) &= 0 \end{aligned} \tag{4.20}$$

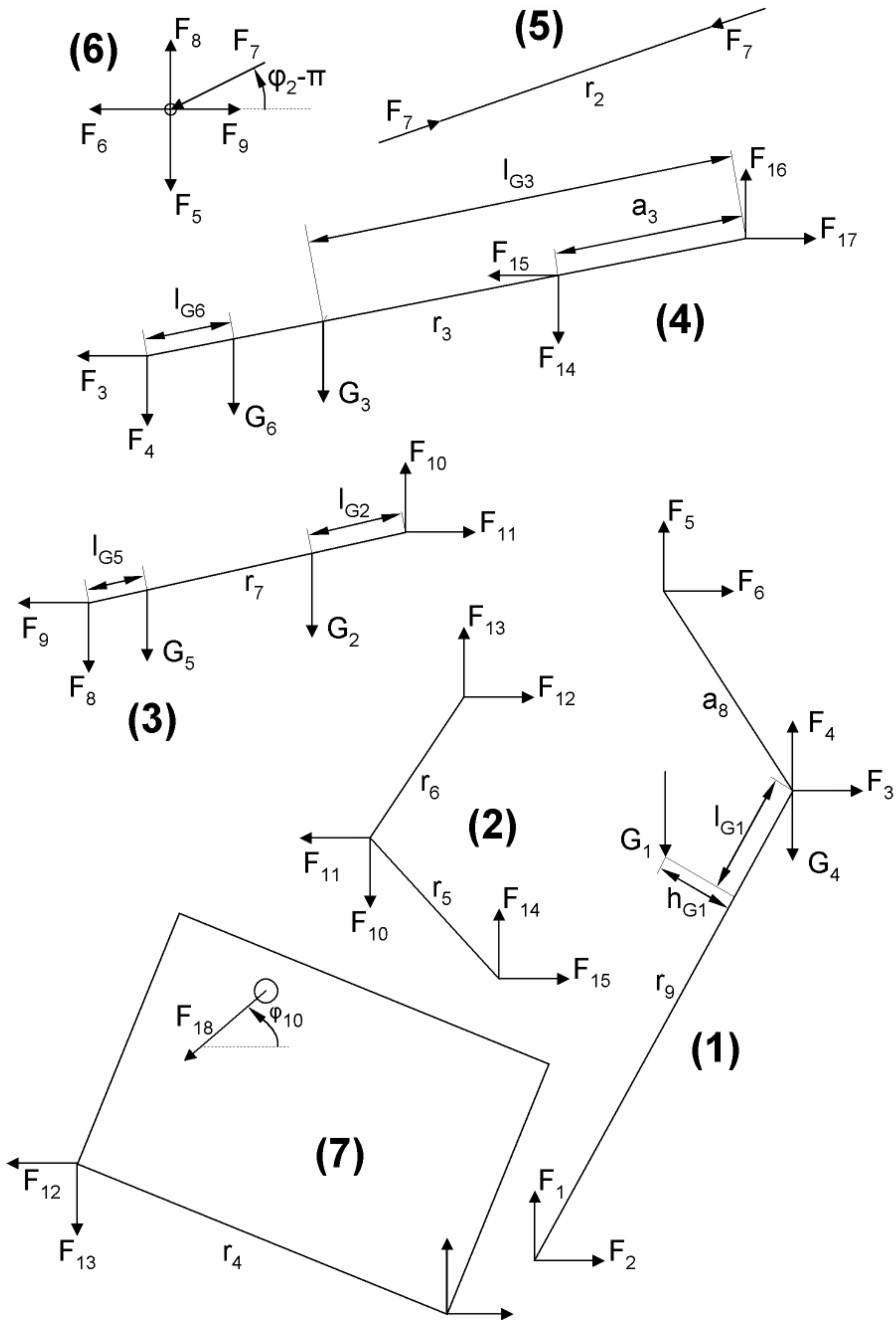

Figure 4.7: free body diagram

Equations for body (3):

$$-F_9 + F_{11} = 0 \tag{4.21}$$

$$-F_8 + F_{10} = G_2 + G_5 \tag{4.22}$$

$$F_8 r_7 \cos\phi_7 - F_9 r_7 \sin\phi_7 = -G_2 l_{G2} \cos\phi_7 - G_5(r_7 - l_{G5}) \cos\phi 7 \tag{4.23}$$

The forces F_{16} and F_{17} are of no interest for the model. Hence only the moment balancing equation of body (4) is needed:

$$\begin{aligned} & -F_4 r_3 \cos\phi_3 - F_{14}(a_3 \cos\phi_3 + b_3 \sin\phi_3) \\ & + F_3 r_3 \sin\phi_3 + F_{15}(a_3 \sin\phi_3 - b_3 \cos\phi_3) = G_3 l_{G3} \cos\phi_3 \\ & \qquad + G_6(r_3 - l_{G6}) \cos\phi_3 \end{aligned} \tag{4.24}$$

Equations for body (6):

$$-F_6 + F_9 + F_7 \cos\phi_2 = 0 \tag{4.25}$$

$$-F_5 + F_8 + F_7 \sin\phi_2 = 0 \tag{4.26}$$

The bearing forces of the plate (7) are not necessary for the model. For that reason only the moment balancing equation needs to be considered. The spring force F_{18} is already known as it can be directly obtained from the length of the spring r_{10}.

$$F_{13} r_4 \cos\phi_4 + F_{12} r_4 \sin\phi_4 = -F_{18} r_1 \sin(\phi_{10} - \phi_1) \tag{4.27}$$

In order to solve these equations the forces on the foot F_1 and F_2 must be given:

$$F_1 = F_1^0 \tag{4.28}$$

$$F_2 = F_2^0 \tag{4.29}$$

This leads to a set of 15 linear equations for 15 forces, F_1 to F_{15}. They can be combined and expressed in the matrix form:

$$\mathbf{mat} \cdot \overrightarrow{F} = \overrightarrow{b} \tag{4.30}$$

The function *LinearSolve[mat,* $\overrightarrow{b}$*]* can be used to solve this equation in MATHEMATICA. It uses different methods depending on what kind of matrix is given (Wolfram

Research 2005*b*). Knowing the forces F_1 to F_{15} the cylinder forces and pressures can be calculated.

4.5.2 Cylinder pressures

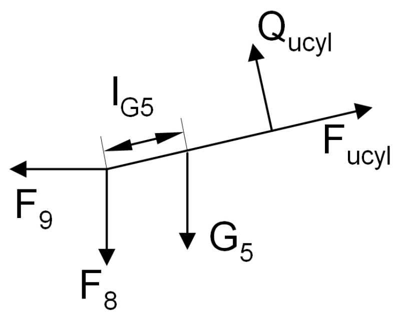

Figure 4.8: upper cylinder piston free body diagram

Figure 4.8 shows the free body diagram of the rod of the upper cylinder. The cylinder force F_{ucyl} can be evaluated as:

$$F_{ucyl} = G_5 \sin\phi_7 + F_9 \cos\phi_7 + F_8 \sin\phi_7 \tag{4.31}$$

The upper cylinder has a power factor of A_{ucyl} =1.7 sq. in. (Clippard Instrument Laboratory 2005*a*). In SI units this is $A_{ucyl} = 1.097 \cdot 10^{-3}\mathrm{m}^2$. This makes the pressure p_7 in [bar]:

$$p_7 = \frac{F_{ucyl}}{A_{ucyl}} = \frac{F_{ucyl}}{1.097 \cdot 10^{-3} \cdot 10^5} = 0.00912(G_5 \sin\phi_7 + F_9 \cos\phi_7 + F_8 \sin\phi_7) \tag{4.32}$$

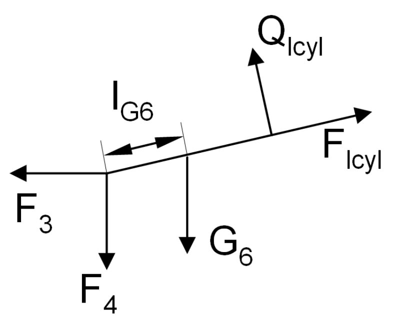

Figure 4.9: lower cylinder piston free body diagram

Figure 4.9 shows the free body diagram of the rod of the lower cylinder. The cylinder force F_{lcyl} can be evaluated as:

$$F_{lcyl} = -(G_6 \sin \phi_3 + F_3 \cos \phi_3 + F_4 \sin \phi_3) \tag{4.33}$$

The lower cylinder has a power factor of A_{lcyl} =1.2 sq. in. (Clippard Instrument Laboratory 2005*b*). In SI units this is $A_{lcyl} = 7.742 \cdot 10^{-4}\mathrm{m}^2$. This makes the pressure p_3 in [bar]:

$$p_3 = \frac{F_{lcyl}}{A_{lcyl}} = \frac{F_{lcyl}}{7.742 \cdot 10^{-4} \cdot 10^5} = -0.0129(G_6 \sin \phi_3 + F_3 \cos \phi_3 + F_4 \sin \phi_3) \tag{4.34}$$

4.6 Weight of the leg

The equations in section 4.5 include forces due to gravity. A leg was measured to have a total mass of 3.7kg. This information alone doesn't help very much as the leg is not a point mass, it is a complex system of a number of parts. The reduction to a point mass is not reasonable as there is relative movement between the parts of the leg.

However, it was not possible to disassemble the whole leg in order to measure the mass and centre of gravity of every single part. A compromise is to include the weights of the major parts.

The weight of the lower part of the leg is represented by G_1. Each cylinder can be represented by two masses, one for the rod and one for the case. For the upper cylinder these weights are G_5 and G_2. For the lower cylinder these weights are G_6 and G_3. The weight of bar (5) in figure 4.7 can be relocated and described by half its weight, G_4. While this relocation does not change the results it simplifies the equations.

The values for all weights and their centres of gravity can be found in table 4.6. All values are estimates, as a complete disassembly and measurement of the leg was not possible.

Table 4.6: weight distribution

weight	value [N]	location
G_1	5.886	l_{G1} =0.165m and h_{G1} =0.03m
G_2	13.2435	l_{G2} =0.09m
G_3	11.772	l_{G3} =0.15m
G_4	1.962	
G_5	0.4905	l_{G5} =0.035m
G_6	0.981	l_{G6} =0.065m

4.7 Summary

The model of a leg is the combination of all the steps and equations described in this chapter. It can be seen as a function for the cylinder pressures depending on the position of the cylinders and the spring and on the forces on the foot of the leg, or:

$$p = p(r_7, r_3, n, h, F_1^0, F_2^0) \tag{4.35}$$

This function is used to optimise the add-on spring mechanism in chapter 6.

Chapter 5

Model Validation

5.1 Overview

The model described in chapter 4 is based on a number of assumptions. For that reason an experiment was performed before using the model for optimisation. This chapter deals with designing and performing such a test in order to verify the accuracy of the model.

Firstly the test arrangement is discussed. The necessary modifications of the model are described, before the results of the test and model are compared.

5.2 Test arrangement

It was not possible to operate the Robug at this stage of the project. For that reason a special test arrangement had to be designed. A leg was taken from the robot and all its valves were opened. It was mounted upside down in order to simulate the weight of the robot by attaching weights to the foot. The lower cylinder was fixed to different lengths r_3.

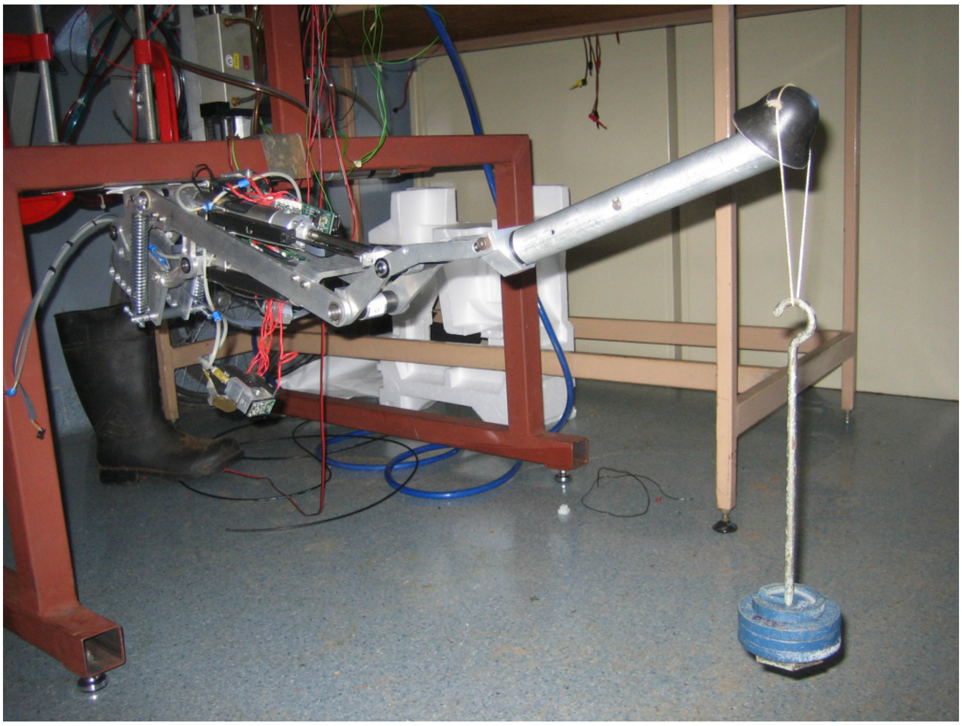

Figure 5.1: test arrangement

A special plate was used which allows the attachment of springs in 8 different positions. These positions can be described in n,h-coordinates and are listed in table 5.1.

Table 5.1: spring positions on the plate used in the test arrangement

position	1	2	3	4	5	6	7	8
n in [m]	0	0.014	0.028	0.042	0.056	0.070	0.084	0.098
h in [m]	0.057	0.057	0.057	0.057	0.057	0.057	0.057	0.057

5.3 Modifications of the model

In the test arrangement the model is mounted upside down. In the model this effect can be reached by changing the direction of gravity, or using negative weights. The weight distribution of the modified model is shown in table 5.2.

Table 5.2: modified weight distribution

weight	value [N]	location
G_1	-5.886	l_{G1} =0.165m and h_{G1} =0.03m
G_2	-13.2435	l_{G2} =0.09m
G_3	-11.772	l_{G3} =0.15m
G_4	-1.962	
G_5	-0.4905	l_{G5} =0.035m
G_6	-0.981	l_{G6} =0.065m

The plates to mount the springs are included by setting the height h to $h = 0.057$m and by expressing the length n as a function of the spring position k:

$$n(k) = 0.014(k-1)\text{m for } k = 1, 2, ..., 8 \tag{5.1}$$

Finally the kinetic boundary conditions need to be modified. The original model assumed both foot forces F_1 and F_2 to be known (See equations 4.28 and 4.29). The aim of the modified model is to calculate the weight that needs to be applied depending on a certain position of the leg and springs.

As the valves of the upper cylinder were removed, the first boundary condition is that the pressure in the upper cylinder equals 0. Using equation 4.31 that means:

$$F_9 \cos\phi_7 + F_8 \sin\phi_7 = -G_5 \sin\phi_7 \tag{5.2}$$

The weights only apply a vertical force on the foot. So the second boundary condition is that the horizontal force component F_2 become 0.

$$F_2 = 0 \tag{5.3}$$

5.4 Comparison of model and experiment

Table 5.3: lower cylinder fixed at $r_3 = 0.291$m, spring located in position $k = 1$

r_7 [mm]	measured weight [kg]	simplified model [kg]	model [kg]
229	3.9	4.5	3.50
231	3.6	4.6	3.49
235	3.4	4.7	3.47
241	3.2	4.8	3.41
259	2.7	5.2	3.10
273	2.2	5.8	2.70

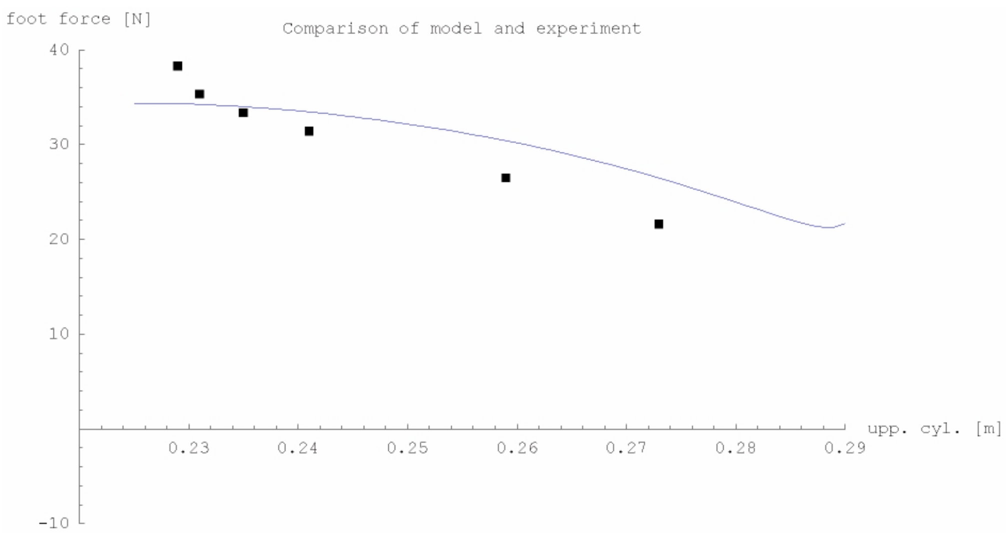

Figure 5.2: comparison of test and model for $r_3 = 0.291$m and the springs located in position 1

The tests were performed before the modified model was evaluated. A string was used to fix the lower cylinder to different lengths. Weights were attached to the foot which caused the leg to shift to a different position. The position was measured for each weight load.

Table 5.4: lower cylinder fixed at $r_3 = 0.287$m, spring located in position $k = 3$

r_7 [mm]	measured weight [kg]	simplified model [kg]	model [kg]
228	2.4	3.3	2.25
231	2.2	3.4	2.25
253	1.9	4.1	2.14
272	1.2	5.1	1.78
278	0.9	6.0	1.58
288	0.0	15.6	0.72

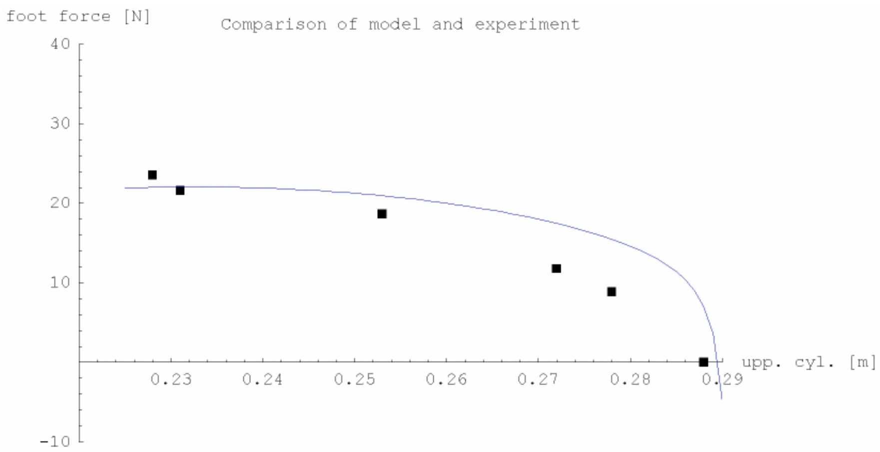

Figure 5.3: comparison of test and model for $r_3 = 0.287$m and the springs located in position 3

The tables in this section list the test data and corresponding model results. After the tests the modified model was used for the leg positions that were found in the tests. In order to compare the calculated foot forces with the attached masses, the foot forces in the model were transformed into masses by using the formula $F = mg$ where $g = 9.81$m/s on earth. In the figures that are used to visualise the data in the tables, the masses are transformed into forces.

Table 5.5: lower cylinder fixed at $r_3 = 0.287$m, spring located in position $k = 5$

r_7 [mm]	measured weight [kg]	simplified model [kg]	model [kg]
227	1.0	2.0	1.00
265	0.9	3.5	0.89
281	0.7	5.9	0.45
289	0.0	19.8	-1.25

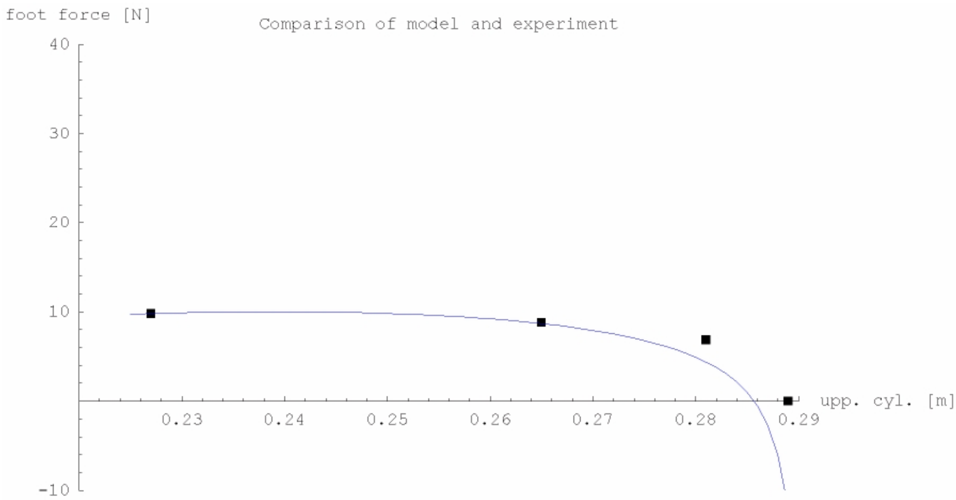

Figure 5.4: comparison of test and model for $r_3 = 0.287$m and the springs located in position 5

The tables include a fourth column that represents a model that does not include the weight of the leg. This is done to examine whether or not the weight of the leg can be considered negligible. Such a model can be easily derived from the modified model by setting $G_1 = G_2 = G_3 = G_4 = G_5 = G_6 = 0$. The test results clearly indicate that it is necessary to include the weight of the leg. The results of the simplified model are not consistent with the test results. In the case of small r_3 values, the necessary attached mass actually increases, while the test shows a decrease.

Table 5.6: lower cylinder fixed at $r_3 = 0.336$m, spring located in position $k = 1$

r_7 [mm]	measured weight [kg]	simplified model [kg]	model [kg]
286	0.0	2.0	0.09
275	0.6	2.3	0.73
270	0.9	2.4	0.97
264	1.2	2.6	1.23
253	1.5	2.9	1.65
246	1.8	3.0	1.90
237	2.2	3.2	2.21
229	2.6	3.4	2.51

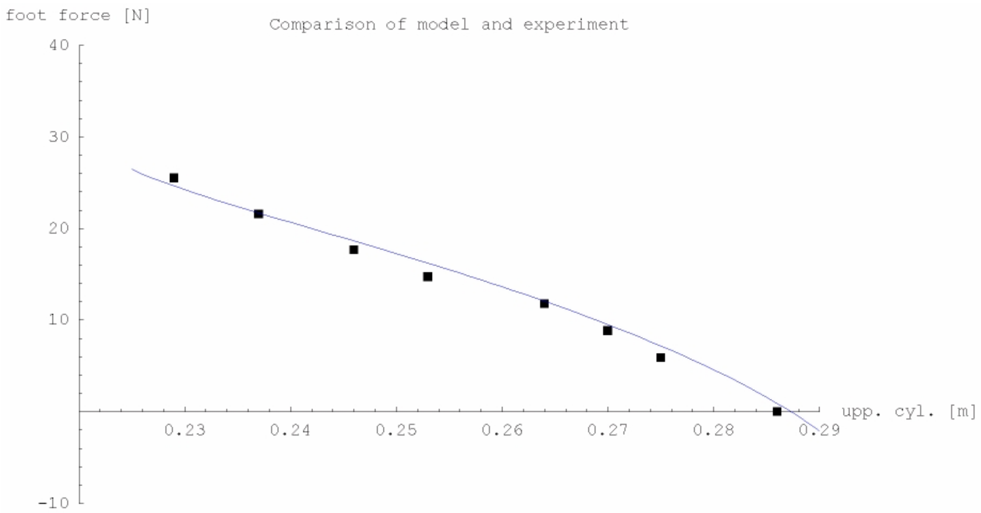

Figure 5.5: comparison of test and model for $r_3 = 0.336$m and the springs located in position 1

The accuracy of this model is a lot better. The average of the absolute values of the differences between the model and the test result is 0.16kg. A closer look at the tables reveals even more. Tests were done for different areas within the whole range of motion. The results clearly indicate that the deviation differs depending on the position.

Table 5.7: lower cylinder fixed at $r_3 = 0.336$m, spring located in position $k = 3$

r_7 [mm]	measured weight [kg]	simplified model [kg]	model [kg]
280	0.0	1.7	0.04
265	0.6	1.9	0.59
253	0.9	2.1	0.92
241	1.2	2.3	1.20
228	1.5	2.4	1.52

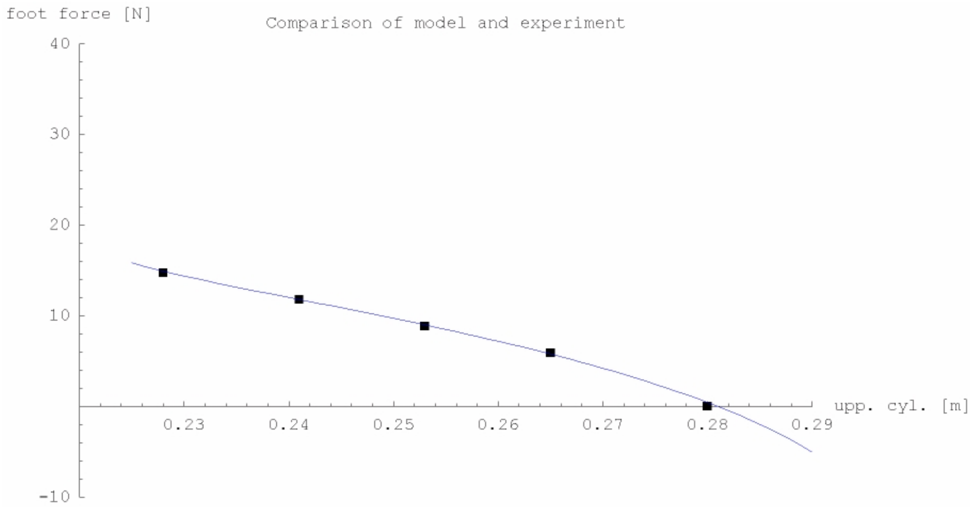

Figure 5.6: comparison of test and model for $r_3 = 0.336$m and the springs located in position 3

The difference between model and test is especially large for small values of r_3. Looking only at values of $r_3 \geq 0.300$m, the average of the absolute values of the differences between the model and the test becomes 0.063kg. This can be clearly seen in the figures in this section. The dots represent the tests, the continuous graphs represent the model.

Table 5.8: lower cylinder fixed at $r_3 = 0.336$m, spring located in position $k = 5$

r_7 [mm]	measured weight [kg]	simplified model [kg]	model [kg]
275	0.0	1.5	-0.05
259	0.2	1.5	0.25
249	0.4	1.5	0.39
238	0.5	1.5	0.52

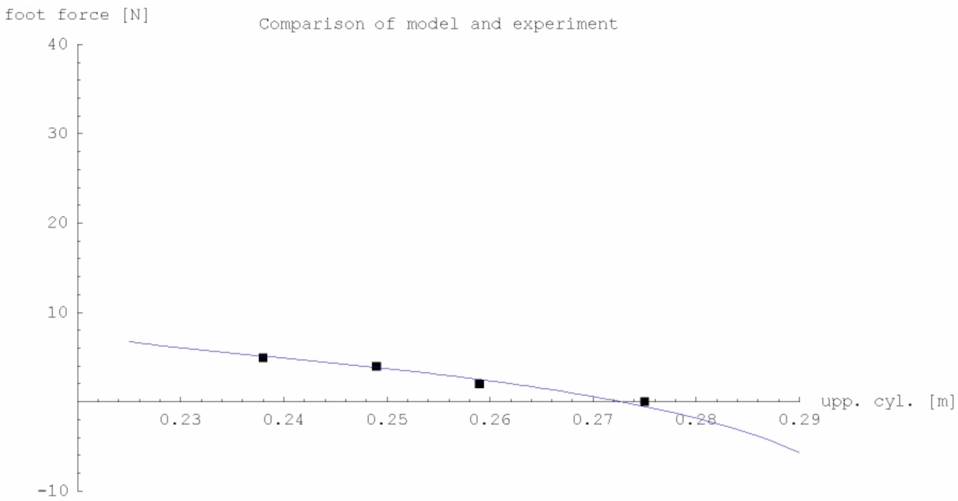

Figure 5.7: comparison of test and model for $r_3 = 0.336$m and the springs located in position 5

While the model is very accurate for medium to large values of r_3, it needs to be treated carefully for large values of r_3. For that part of the range of motion it is difficult to tell whether the model or the test arrangement is inaccurate. Slightly wrong measurements of the parts of the leg could affect the model. Or it could be the test arrangement as for small values of r_3 the foot stands close to the hip causing smaller lever arms and due to the rounding of the foot the weights couldn't be attached right at the tip of the foot.

Table 5.9: lower cylinder fixed at $r_3 = 0.381$m, spring located in position $k = 1$

r_7 [mm]	measured weight [kg]	simplified model [kg]	model [kg]
285	0.0	1.3	0.12
277	0.4	1.6	0.46
265	0.8	2.0	0.94
256	1.2	2.3	1.29
246	1.6	2.7	1.71
239	2.0	3.0	2.04

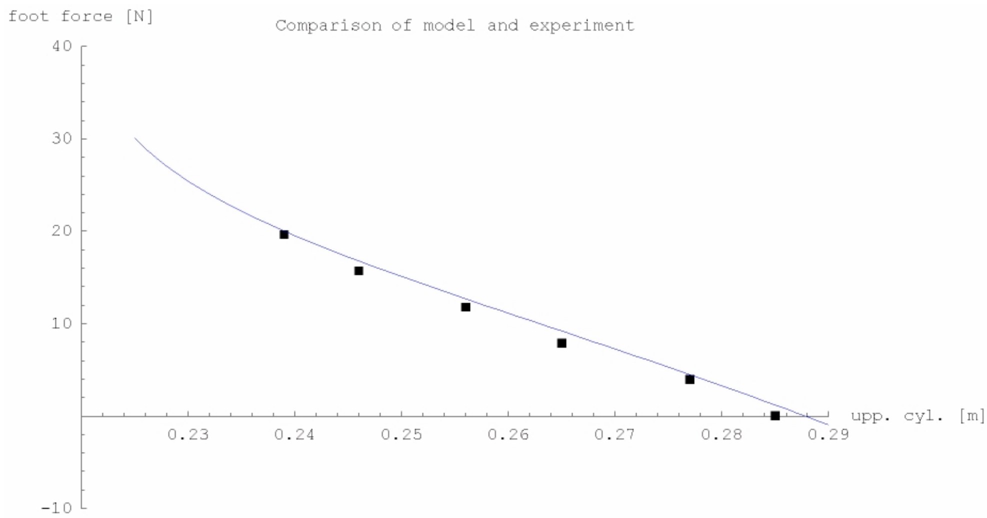

Figure 5.8: comparison of test and model for $r_3 = 0.381$m and the springs located in position 1

The last parameter to test was the spring position. Different spring positions were used in the test arrangement for the same position of the upper cylinder. The tests show that the modelling of the springs and their positions is accurate as no association can be seen in the tables between an increased deviation and a particular spring position.

Table 5.10: lower cylinder fixed at $r_3 = 0.381$m, spring located in position $k = 4$

r_7 [mm]	measured weight [kg]	simplified model [kg]	model [kg]
273	0.0	1.2	0.08
264	0.2	1.3	0.27
254	0.4	1.5	0.48
245	0.6	1.7	0.66
237	0.9	1.8	0.85

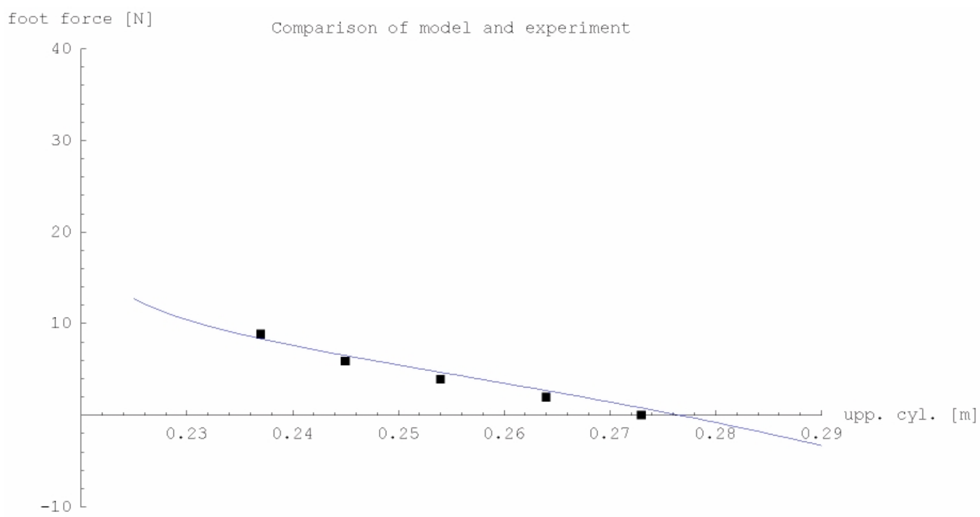

Figure 5.9: comparison of test and model for $r_3 = 0.381$m and the springs located in position 4

Table 5.11: lower cylinder fixed at $r_3 = 0.381$m, spring located in position $k = 4$

r_7 [mm]	measured weight [kg]	simplified model [kg]	model [kg]
267	0.0	1.1	0.05
255	0.2	1.3	0.23
238	0.4	1.4	0.47

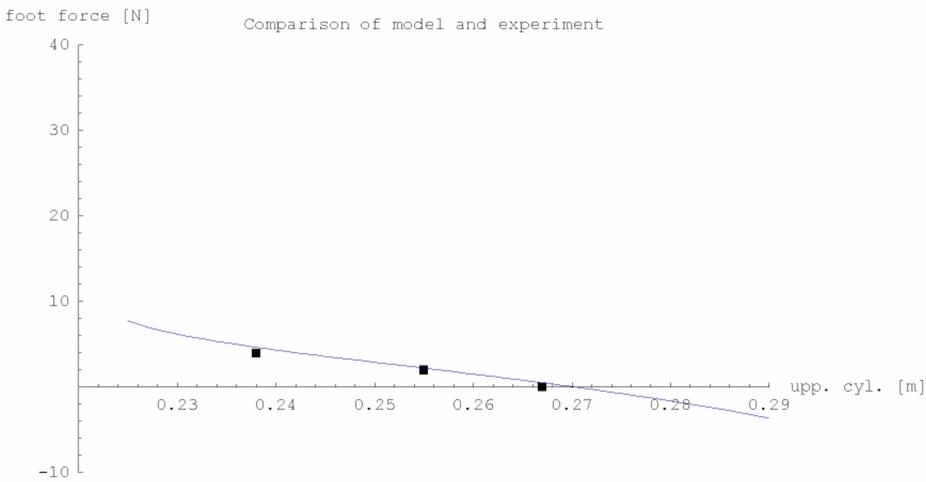

Figure 5.10: comparison of test and model for $r_3 = 0.381$m and the springs located in position 5

5.5 Summary

The model that includes the weight of the leg is accurate, especially for large values of r_3. For small values of r_3 the model should be treated with care. Different spring positions do not affect the accuracy of the model.

Chapter 6

Design of the mechanism

6.1 Overview

This chapter deals with the design of the spring mechanism by using the model of the leg. Parameters that could be changed are the spring coefficient, the unstressed length and the position in which the springs are mounted on the plates. The aim is to find a configuration that allows the Robug to be operated on the 6-bar air supply that is available at the USQ lab.

One attempt is to minimise the pressure in the cylinders over the whole range of motion. A second attempt is to define a typical range of motion and find a spring configuration that allows the Robug to operate at an acceptable pressure level.

The last section deals with the predicted behaviour of the leg.

6.2 Overall Optimisation

The first attempt was to find the spring position that minimises the pressure in the cylinders for the whole range of motion. The range of motion for the cylinders is $0.225\text{m} \leq r_7 \leq 0.280\text{m}$ and $0.285\text{m} \leq r_3 \leq 0.380\text{m}$.

It is not possible to calculate the derivative for the pressures because of the model being numerical. For that reason a grid was put over the range of motion and the pressures were calculated for every grid point. The highest calculated pressure is the pressure needed to use the whole range of motion of the robot.

The first problem with this approach is that it takes a considerable amount of time to calculate the pressures for every grid point. For a grid that uses a point every millimeter 5225 points need to be evaluated for each spring configuration.

The second and main problem is that it is not possible to find a position where the needed pressure is below 10bar. For that reason the results of this approach are worthless for the design of the spring mechanism. However, they do show that it is not possible to use the whole range of motion of the Robug with a 6bar air supply.

6.3 Limited range of motion approach

6.3.1 Typical range of motion

As it is not possible to use the whole range of motion, it is necessary to define a typical range of motion that will normally be used. The robot needs to be able to stand up and walk. In order to prevent feet sliding over the ground it is desirable that the feet do not move horizontally. To prevent horizontal movement an association between r_3 ad r_7 needs to be found. This limits the degrees of freedom to 1. For $0.235\text{m} \leq r_7 \leq 0.270\text{m}$ a good approximation is:

$$r_3 = 14.071\text{m}^{-1} r_7^2 - 6.345 r_7 + 1.028\text{m} \tag{6.1}$$

which makes $0.314\text{m} \leq r_3 \leq 0.341\text{m}$. A benefit of this range of motion is the avoidance of those small r_3 values, for which model and test didn't match. An animation of this range of motion can be found on the attached CD-ROM.

6.3.2 Types of motion

There are three different types of motion for the Robug. They differ in the number of legs used simultaneously and in the forces on the feet.

- The first one is **standing up**. This means lifting the torso off the ground. All 8 legs can be used to stand up. The mass of a leg was measured to be 3.7kg, and the torso 22.2kg. This makes the total mass 51.8kg. Distributing the weight equally on all 8 legs, the foot force F_1 becomes:

$$F_1 = \frac{51.8}{8} \cdot 9.81 = 63.52\text{N} \tag{6.2}$$

  For typical conditions the horizontal foot force can be assumed to be $F_2 = 0$N.

- The second one is **standing**. In order to walk the robot must be able to stand on a number of legs while the other legs are shifted. Typically the Robug could stand on 6 legs (3 on each side) while two legs are up in the air. Distributing the weight equally on 6 legs, the foot force becomes:

$$F_1 = \frac{51.8}{6} \cdot 9.81 = 84.7\text{N} \tag{6.3}$$

  Once again it can be assumed that $F_2 = 0$N. A typical standing position is $r_7 = 0.265$m. Using equation 6.1, r_3 becomes 0.3347m.

- The final one is **lifting a leg** off the ground. This needs to be done to take a step. The starting position is the standing position. In order to lift the leg a reasonable amount off the ground the range of motion taken into account is $0.265\text{m} \geq r_7 \geq 0.250\text{m}$. Again equation 6.1 is used to calculate r_3.

  When lifted, the foot does not touch the ground, and therefore $F_1 = F_2 = 0$N.

6.3.3 Selection of a position

The approach is to find the position for the existing springs that minimises the pressures for the previously described motions. If the results are not good enough springs with different parameters could be tried.

The first step is to program a module $maxp(n, h)$ which calculates the largest pressures that occur over the limited range of motion depending on the spring position. The source code of this module can be found in appendix B.5.

The internal variable *zylmax* describes the maximum pressure. The pressures are calculated for all three types of motion. Using a step size of 2mm, 25 points need to be evaluated. At each point the absolute cylinder pressures $z3$ and $z7$ are compared with the absolute value of *zylmax*. If one of them is larger than the absolute value of *zylmax*, *zylmax* is assigned a new value. Absolute values are used because the pressures can be both negative and positive as the cylinders are two-way cylinders.

The additional variables *zyl7pos*, *zylnummer* and *art* are used to store additional information about in which cylinder the maximum pressure appears, at what position and during wich type of motion.

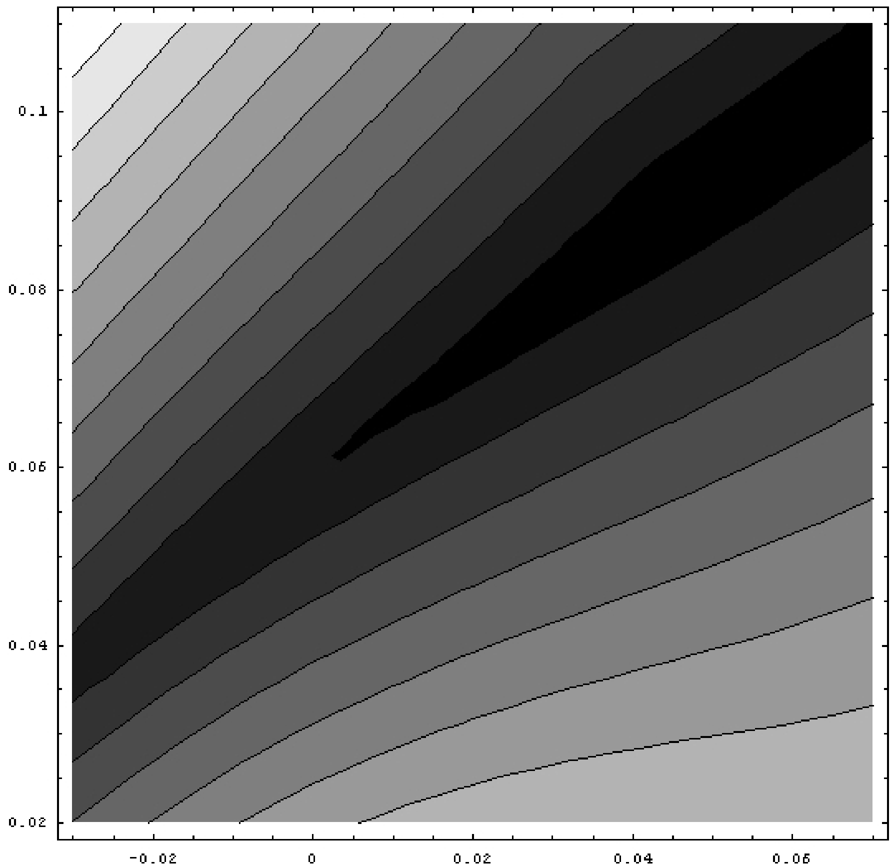

Figure 6.1: plot of the absolute value of $maxp$ for $-0.030\text{m} \leq n \leq 0.070\text{m}$ and $0.020\text{m} \leq h \leq 0.110\text{m}$.

The next step is to examine the maximum pressures for different values of n and h. Having the possible size of the plates in mind, the area which is searched for a spring position will be limited to $-0.030\text{m} \leq n \leq 0.070\text{m}$ and $0.020\text{m} \leq h \leq 0.110\text{m}$.

Figure 6.1 is a contour plot of $|maxp|$. The black strip indicates the area of the smallest absolute values of $maxp$. The centre of the black strip can be approximated by a linear function:

$$n(h) = 1.53h - 0.0908\text{m} \tag{6.4}$$

Using equation 6.4 $maxp(n, h)$ can be plotted for $0.020\text{m} \leq h \leq 0.110\text{m}$ as shown in figure 6.2.

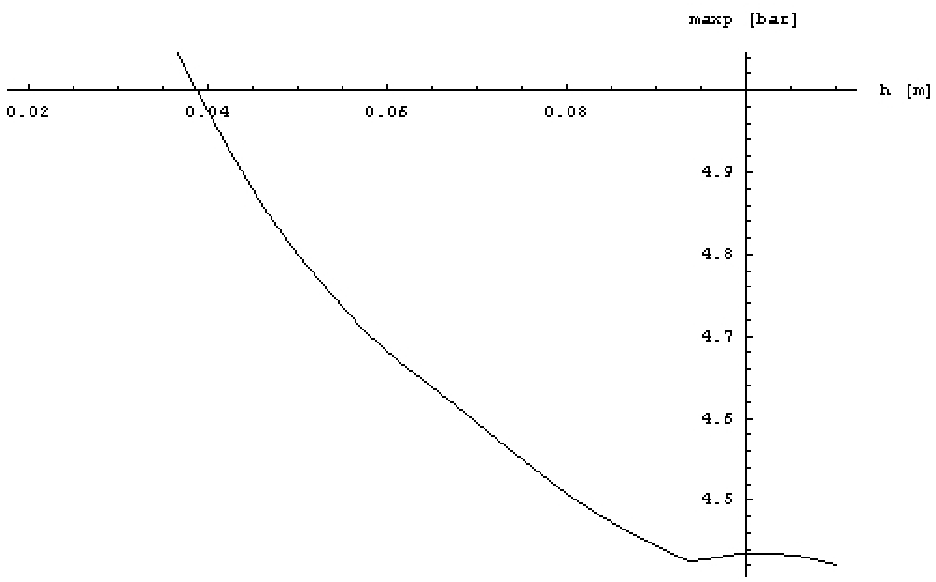

Figure 6.2: plot of the absolute value of $maxp$ using the association shown in equation 6.4.

According to the plot, the position that minimises the necessary pressure supply is $h \approx 0.093\text{m}$ and $n \approx 0.051$. However there is a difference between a mathematical result and a good engineering solution. A few more things need to be taken into consideration before choosing a position for the springs.

One thing that needs to be considered is the force that is necessary to attach the springs to the plates. The way the mechanism is designed the length r_{10} of the springs is always longer than the lengths when no external forces are applied. This means that the springs need to be stressed in order to get them into position for attaching them to the plates. The force necessary to stretch them that much may not be too high. This force is also the force that will always remain in the springs as long as they are attached to the legs. r_{10} is at a minimum when $r_7 = 0.280$m and $r_3 = 0.285$m. This is the position in which the springs should be installed.

Another thing that needs to be considered is the maximum stress of the springs. If it is too large the forces could become so high that the mechanism breaks. The spring force is largest for $r_7 = 0.225$m and $r_3 = 0.285$m.

Using equation 6.4 both the minimum and maximum spring force can be plotted for different spring positions as shown in figure 6.3.

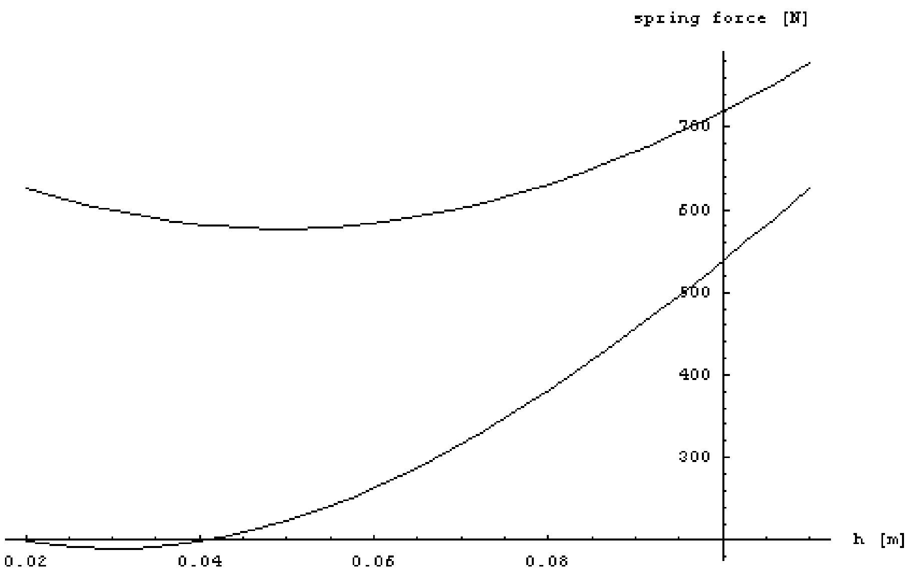

Figure 6.3: plot of the minimum and maximum spring force depending on the spring position.

Figures 6.2 and 6.3 show that there is no such thing as the 'best' position to attach the springs to the plates. An increase in height h improves the maximum of the cylinder pressures, but the price to pay is a higher spring force.

A compromise needs to be made that limits the cylinder pressures and does not result in too large spring forces. A good value to select is $h = 0.060$m. Using equation 6.4 makes $n = 0.001$m. This position limits the maximum pressure to 4.7bar. It occurs in cylinder r_7 at the highest point the leg is lifted to in the described range of motion.

4.7bar is a good value as the compressor at the USQ laboratory produces 6 bar. That gives a safety factor of 1.28 which should compensate for dynamic effects and friction that were not considered in the model.

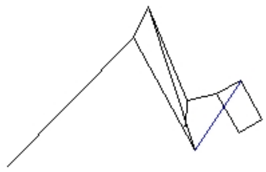

Figure 6.4: position with the largest spring force value

With this position the combined spring force is limited to 584N. Two similar springs are used in a parallel design, so the maximum force in each spring becomes 292N.

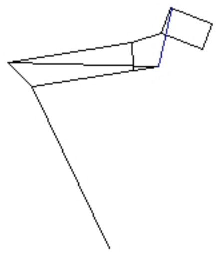

Figure 6.5: position with the smallest spring force value

The smallest force in each spring is 131N. It needs to be applied in order to attach each spring. A normal person is able to apply a force of 131N, so this is an acceptable value.

6.4 Summary

It is not possible to design a spring mechanism that allows use of the whole range of motion with a 6bar air supply. That is why a typical range of motion is defined in equation 6.1.

Three types of motion were considered: standing up, standing and lifting a leg off the ground. A good position to limit the maximum pressures is $n = 0.001$m and $h = 0.060$m.

Chapter 7

Manufacture and Assembly of the exoskeletal system

7.1 Chapter Overview

This chapter deals with the manufacturing of the add-on spring mechanism. Drawings need to be made of the necessary parts, they need to be manufactured and assembled.

7.2 Necessary parts

The mechanism developed in chapter 6 uses the springs and bolts that already existed previously to this project. As a result the only parts that need to be manufactured are the plates to which the springs will be attached.

The parts need to have the correct holes allowing them to be assembled with the rest of the leg. Figures 7.1 and 7.2 show technical drawings of the two plates.

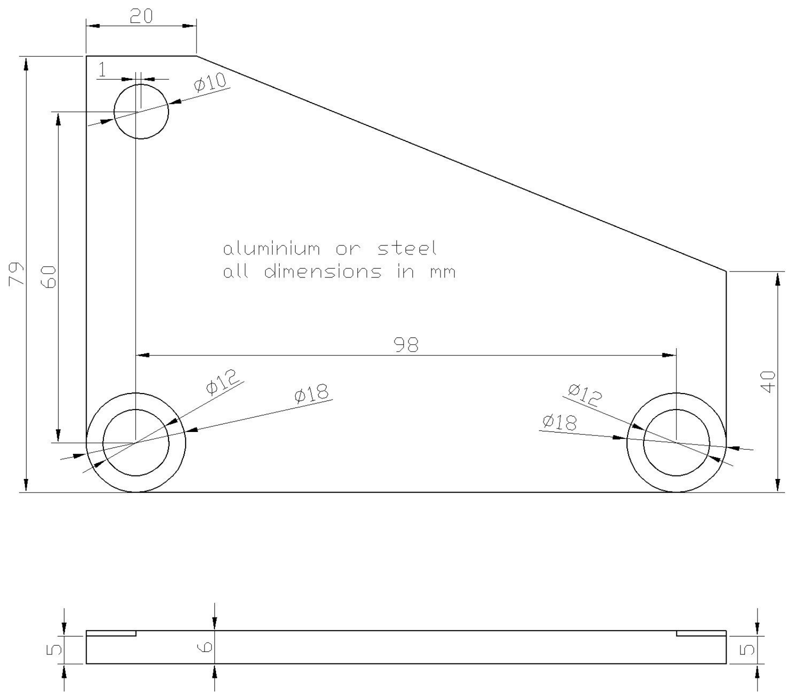

Figure 7.1: technical drawing of the first plate

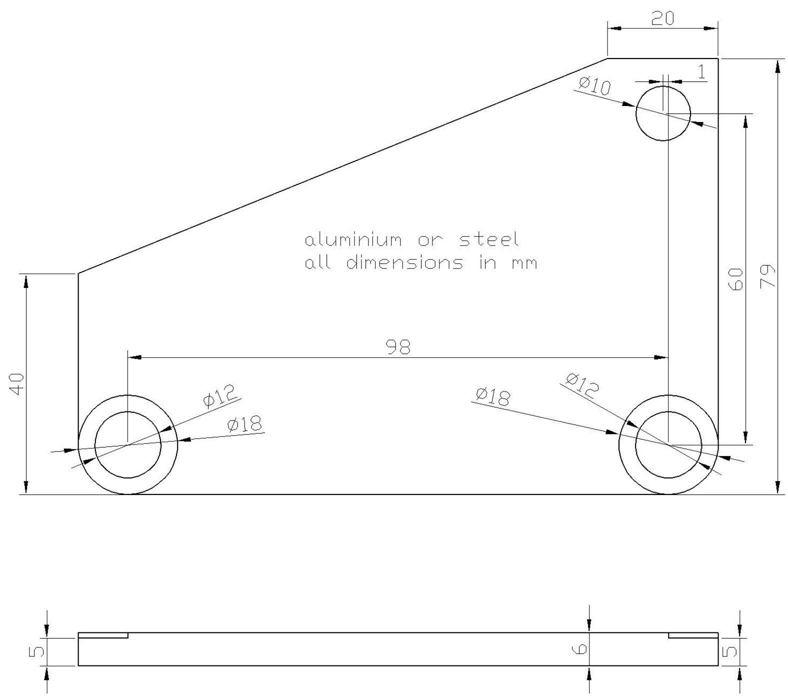

Figure 7.2: technical drawing of the second plate

7.3 Production and assembly

It was possible to have the plates manufactured at the Mechanical Workshop at the University of Southern Queensland. However, the existing manufactured plates have the holes for the springs in the wrong position.

This is due to an error in the model of the leg. This error was only found after the work request form had already been submitted. When the error was corrected and the new position for the springs was found not enough time was left to manufacture another set of plates.

However, the plates that already exist are very similar to the ones designed in chapter 6. The first spring position is $n = 0.000$m and $h = 0.0057$m compared with $n = 0.001$m and $h = 0.0060$m. This difference is so small that it is not absolutely necessary to have the new plates manufactured.

The existing plates are already assembled, so no additional assembly had to be done. Figure 7.3 shows a photo of the assembled mechanism.

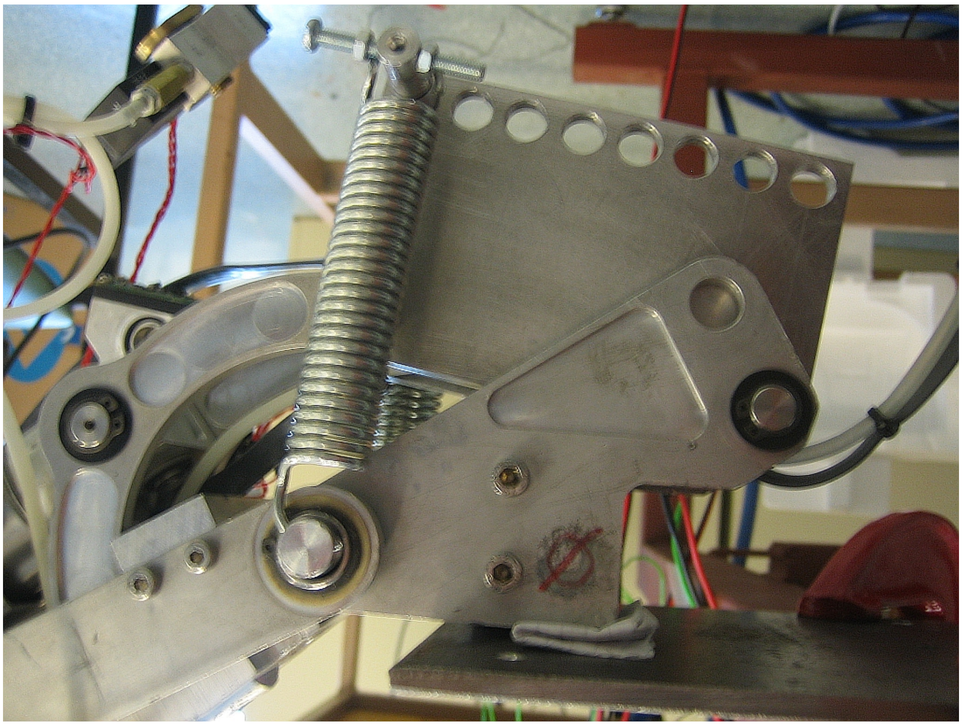

Figure 7.3: spring mechanism

7.4 Summary

The new plates were designed, but due to a modelling error plates with incorrect positions were manufactured. However, the existing plates have a position similar to the one on the new plates.

Chapter 8

Further analysis of the final mechanism

8.1 Overview

After defining the parameters of the mechanism further analysis needs to be done. In chapter 6 the maximum pressure for the typical range of motion was found to be 4.7 bar. However, what exactly will the pressures be like for the three different types of motion?

So far the dynamic equilibrium was calculated for each position, but it was not checked whether the equilibrium is stable. This is very important because if a position was unstable, the leg would automatically shift to the closest stable position. This could make it impossible to use the Robug. Another danger is that positions could exist where the leg locks up, where it is not possible to move the leg by changing the pressures in the cylinders. If such positions exist they need to be avoided.

The above mentioned aspects will be investigated for both the typical range of motion and the whole range of motion.

8.2 Estimated pressures

8.2.1 Typical range of motion

Maps can be plotted that show the pressures in both cylinders for the three different types of motion.

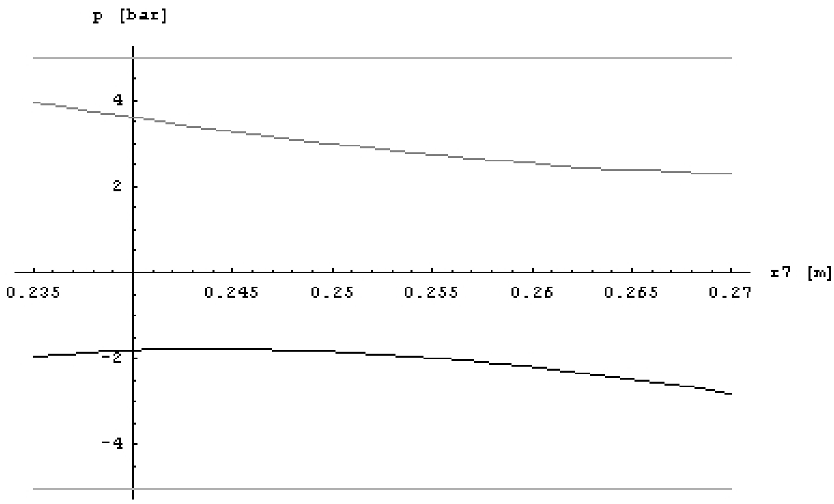

Figure 8.1: pressures in cylinders r_7 (black) and r_3 (gray) when standing up for the typical range of motion, $n = 0.001$m and $h = 0.060$m. The horizontal lines indicate ± 5bar.

Figure 8.1 shows the pressures when standing up. The maximum pressure is approximately 4.0bar. This corresponds to a safety factor of 1.5. It is larger than the overall safety factor of 1.28 which is good because the dynamic forces of the torso need to be compensated for when it is lifted up.

The typical standing position was assumed to be $r_7 = 0.265$m. Figure 8.2 shows that the robot should be able to stand on just 6 legs at any point of the typical range of motion.

Figure 8.3 shows the pressures when a leg is lifted off the ground. The pressure in cylinder r_3 becomes almost 0 as only the weight of the lower part of the leg rests on it. The higher the leg is lifted the larger is the pressure in cylinder r_7. For a wide range of motion the pressure is below 5 bar, so it is not a problem to lift the leg high enough to avoid obstacles.

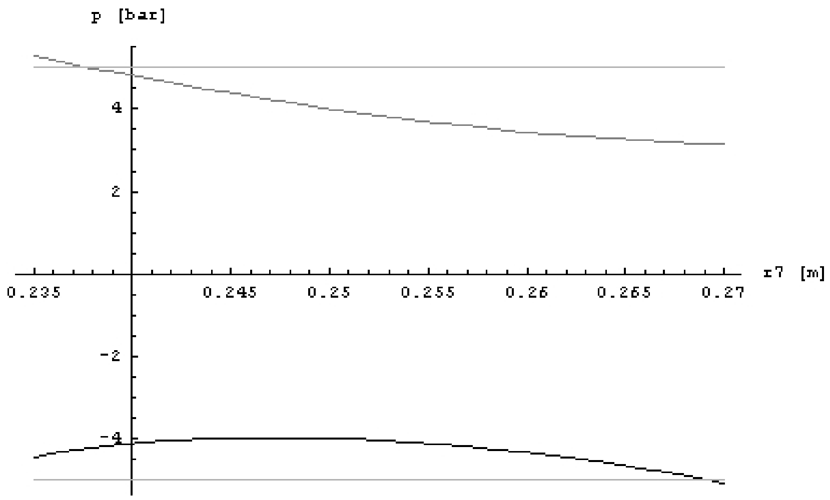

Figure 8.2: pressures in cylinders r_7 (black) and r_3 (gray) when standing for the typical range of motion, $n = 0.001$m and $h = 0.060$m. The horizontal lines indicate ±5bar.

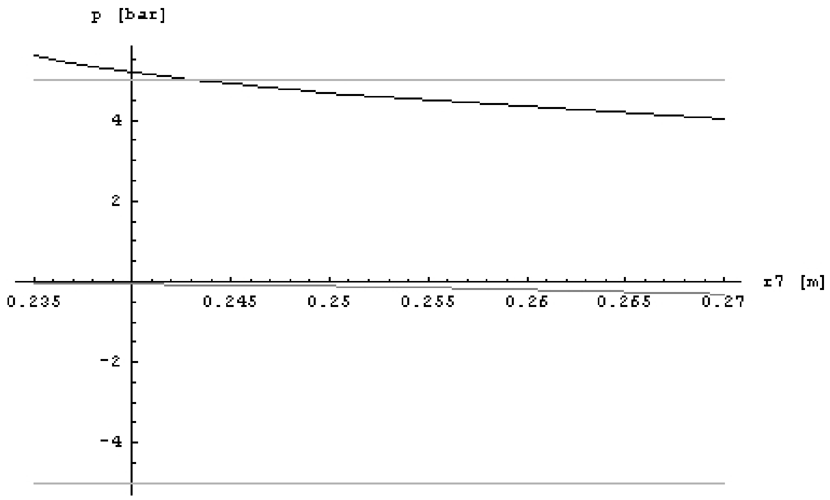

Figure 8.3: pressures in cylinders r_7 (black) and r_3 (gray) when lifting a leg for the typical range of motion, $n = 0.001$m and $h = 0.060$m. The horizontal lines indicate ±5bar.

8.2.2 Whole range of motion

Knowing that it will be possible to operate the Robug on a 6bar air supply using the the typical range of motion the next question is how much of the whole range of motion is accessible?

Three dimensional plots can be created. Each plot shows the pressure of a cylinder for a certain type of motion. It depends on the positions r_3 and r_7.

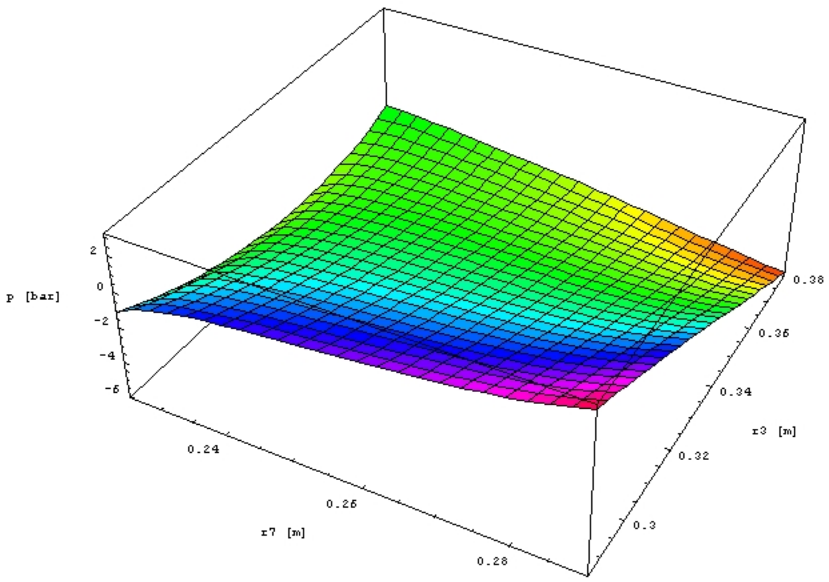

Figure 8.4: pressure in cylinder r_7 when standing up. $n = 0.001$m and $h = 0.060$m.

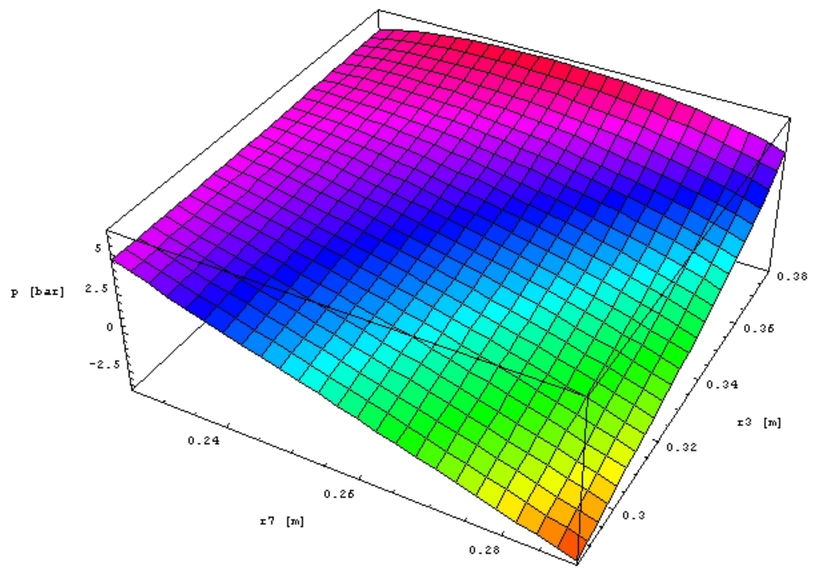

Figure 8.5: pressure in cylinder r_3 when standing up. $n = 0.001$m and $h = 0.060$m.

Figures 8.4 and 8.5 show that almost the whole range of motion will be accessible when Robug IV is standing up. The highest pressures are necessary for large values of r_3, that is, when the feet stand far away from the torso.

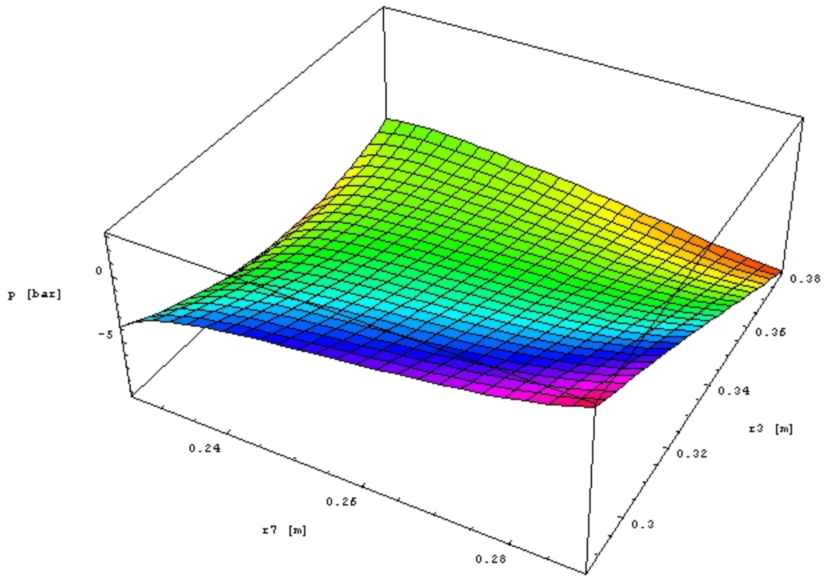

Figure 8.6: pressure in cylinder r_7 when standing. $n = 0.001$m and $h = 0.060$m.

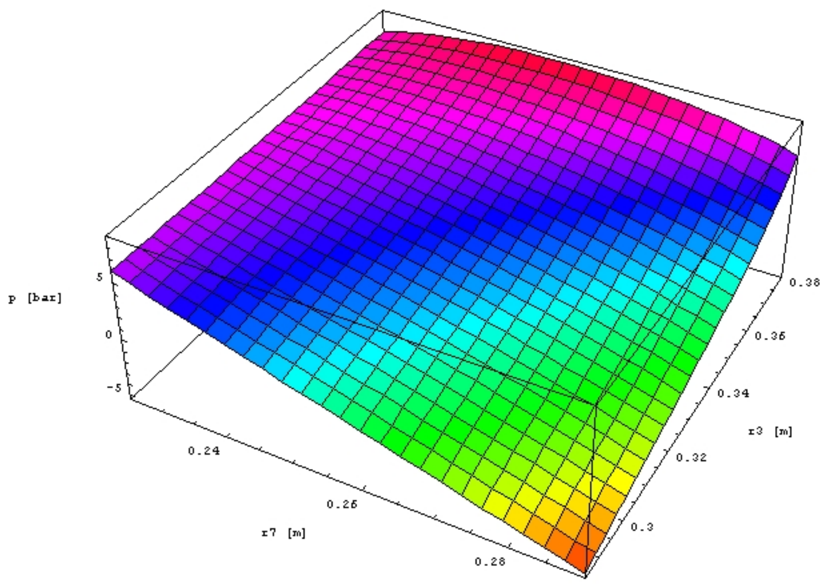

Figure 8.7: pressure in cylinder r_3 when standing. $n = 0.001$m and $h = 0.060$m.

The pressures that are necessary to stand on 6 legs are similar to those when standing up as figures 8.6 and 8.7 show. A wide range of motion is accessible, which can be approximately described by $r_3 < 0.35$m.

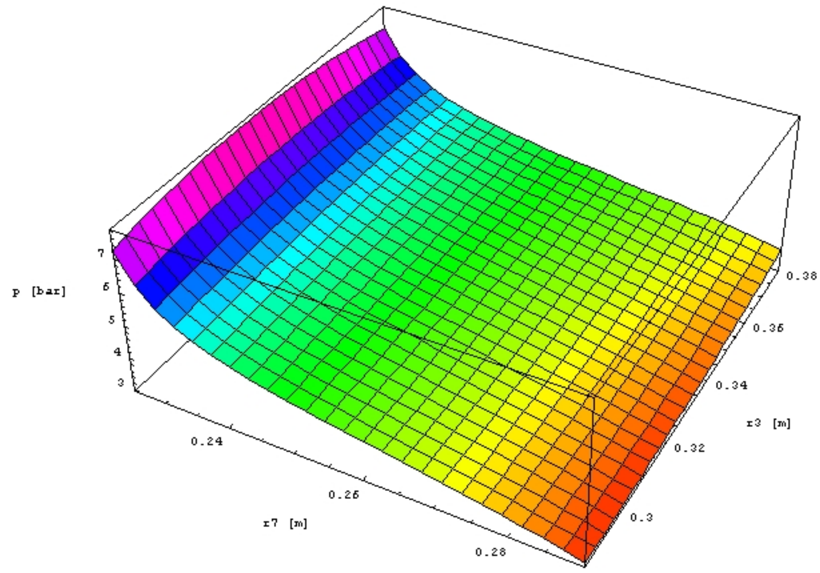

Figure 8.8: pressure in cylinder r_7 when lifting a leg off the ground. $n = 0.001$m and $h = 0.060$m.

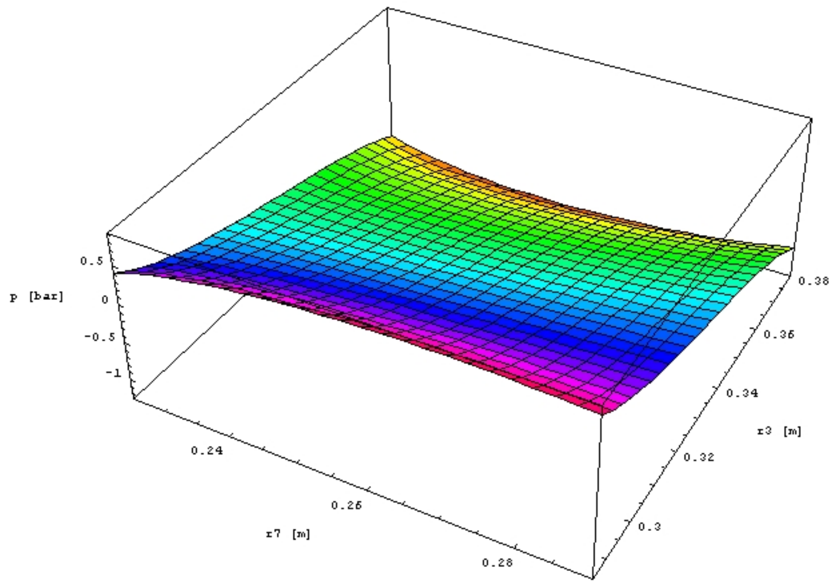

Figure 8.9: pressure in cylinder r_3 when lifting a leg off the ground. $n = 0.001$m and $h = 0.060$m.

The necessary pressure in cylinder r_3 is as expected very low when lifting a leg off the ground as figures 8.4 and 8.5 show. The whole range of motion is available to r_3 for any value of r_7, but r_7 is limited approximately to $r_7 > 0.24$m.

8.3 Stability

A good analogy for the importance of stability is a ball on top of a hill. It will roll down to one side or the other, although the top of the hill is a horizontal point. This is because although the ball is in a state of equilibrium on top of the hill, this equilibrium is unstable.

Something similar could exist for the cylinders of the robug. Figure 8.2 shows an extreme value for the pressure in cylinder r_7, but does that mean that this position is unstable?

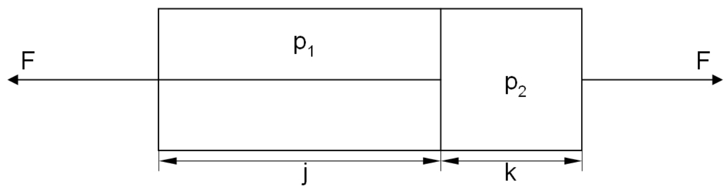

Figure 8.10: schematic drawing of a two-way cylinder

Figure 8.10 shows a schematic drawing of a two-way cylinder. The pressures in the chambers are p_1 and p_2, F is the external force and the area of the piston is A. Assuming A to be the same for both chambers the equilibrium is given by:

$$\frac{F}{A} = p_1 - p_2 \tag{8.1}$$

By defining an external pressure $p_{ex} = F/A$ and an internal pressure $p_{in} = p_1 - p_2$ equation 8.1 can be written as:

$$p_{ex} = p_{in} \tag{8.2}$$

The lengths j and k can be calculated to be $j = r_{i,max} - r_i$ and $k = r_i - r_{i,min}$ where $i = 3, 7$.

Assuming that both valves are closed and that the temperature remains constant for small changes in j and k, figure 8.11 shows a schematic plot of how p_{in} changes with j.

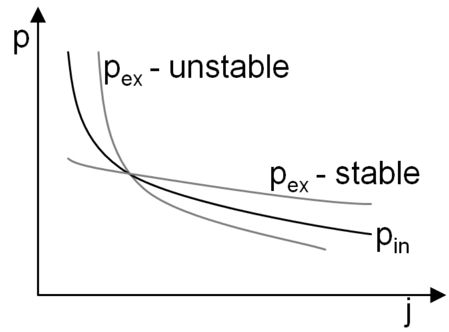

Figure 8.11: difference between a stable position and an unstable one

If $p_{ex} > p_{in}$ for a slightly increased value $j_0+\Delta j$, and if $p_{ex} < p_{in}$ for a slightly decreased value $j_0 - \Delta j$ the position is stable. This is so because, for any small disturbance, the forces change in a way so that the cylinder returns to the balanced position. This means, an equilibrium is stable if:

$$\left.\frac{\mathrm{d}p_{ex}}{\mathrm{d}j}\right|_{j=j_0} > \left.\frac{\mathrm{d}p_{in}}{\mathrm{d}j}\right|_{j=j_0} \tag{8.3}$$

$$\Leftrightarrow -\left.\frac{\mathrm{d}p_{ex}}{\mathrm{d}r_i}\right|_{j=j_0} > \left.\frac{\mathrm{d}p_1}{\mathrm{d}j}\right|_{j=j_0} - \left.\frac{\mathrm{d}p_2}{\mathrm{d}j}\right|_{j=j_0} \tag{8.4}$$

$$\Leftrightarrow -\left.\frac{\mathrm{d}p_{ex}}{\mathrm{d}r_i}\right|_{j=j_0} > \left.\frac{\mathrm{d}p_1}{\mathrm{d}j}\right|_{j=j_0} + \left.\frac{\mathrm{d}p_2}{\mathrm{d}k}\right|_{j=j_0} \tag{8.5}$$

p_{ex} does not exist in the form of a continuous function, so it is not possible to calculate its derivative. But it can be approximated:

$$-\left.\frac{\mathrm{d}p_{ex}}{\mathrm{d}r_i}\right|_{j=j_0} \approx -\frac{p_{ex}(r_{i,0}+\Delta r_i) - p_{ex}(r_{i,0})}{\Delta r_i} = \frac{p_{ex}(r_{i,0}) - p_{ex}(r_{i,0}+\Delta r_i)}{\Delta r_i} \tag{8.6}$$

where Δr_i is a small value, e.g. 0.0001m. Assuming that the valves sit right on the cylinder and are shut and assuming that the temperature is constant, the ideal gas law can be used for p_1:

$$p_1 \cdot j = \frac{R \cdot T \cdot m}{A} = \text{const.} \tag{8.7}$$

This makes the derivative at the point $j = j_0$:

$$\left.\frac{\mathrm{d}p_1}{\mathrm{d}j}\right|_{j=j_0} = -\left.\frac{R \cdot T \cdot m}{j^2}\right|_{j=j_0} = -\frac{p_1(r_{i,0})}{j} = -\frac{p_1(r_{i,0})}{r_{i,max} - r_i} \tag{8.8}$$

The same procedure can be used for p_2:

$$p_2 \cdot k = \frac{R \cdot T \cdot m}{A} = \text{const.} \tag{8.9}$$

$$\Rightarrow \left.\frac{\mathrm{d}p_2}{\mathrm{d}k}\right|_{j=j_0} = -\left.\frac{R\cdot T\cdot m}{k^2}\right|_{j=j_0} = -\frac{p_2(r_{i,0})}{k} = -\frac{p_2(r_{i,0})}{r_i - r_{i,min}} \tag{8.10}$$

Substituting and rearranging the terms in equation 8.5 we get:

$$\frac{p_{ex}(r_{i,0}) - p_{ex}(r_{i,0}+\Delta r_i)}{\Delta r_i} > -\frac{p_1(r_{i,0})}{r_{i,max} - r_i} - \frac{p_2(r_{i,0})}{r_i - r_{i,min}} \tag{8.11}$$

$$\Leftrightarrow \sigma_i = \frac{p_{ex}(r_{i,0}) - p_{ex}(r_{i,0}+\Delta r_i)}{\Delta r_i} + \frac{p_1(r_{i,0})}{r_{i,max} - r_i} + \frac{p_2(r_{i,0})}{r_i - r_{i,min}} > 0 \tag{8.12}$$

This stability condition can be used for both cylinders:

$$\sigma_7 = \frac{p_{ex}(r_7) - p_{ex}(r_7+\Delta r_7)}{\Delta r_7} + \frac{p_1(r_7)}{0.300\mathrm{m} - r_7} + \frac{p_2(r_7)}{r_7 - 0.225\mathrm{m}} \quad > \quad 0 \tag{8.13}$$

$$\sigma_3 = \frac{p_{ex}(r_3) - p_{ex}(r_3+\Delta r_3)}{\Delta r_3} + \frac{p_1(r_3)}{0.380\mathrm{m} - r_3} + \frac{p_2(r_3)}{r_3 - 0.285\mathrm{m}} \quad > \quad 0 \tag{8.14}$$

8.3.1 Typical range of motion

The inequalities 8.13 and 8.14 can be evaluated for the typical range of motion in order to test the stability of each type of motion.

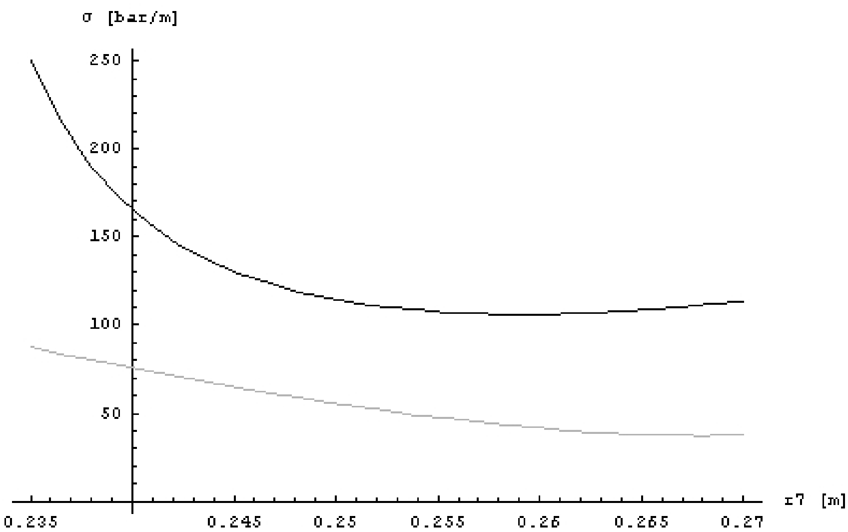

Figure 8.12: stability of cylinder r_7 (black) and cylinder r_3 (grey) when standing up

The pressures p_1 and p_2 are unknown, only their difference $p_{in} = p_{ex}$ is known. A possible configuration is to set the smaller one of p_1 and p_2 to atmospheric pressure, $\approx$ 1bar. This means:

$$\text{For } p_{ex} \geq 0: \qquad p_1 = p_{ex} + 1\text{bar and } p_2 = 1\text{bar} \tag{8.15}$$

$$\text{For } p_{ex} < 0: \qquad p_1 = 1\text{bar and } p_2 = 1\text{bar} - p_{ex} \tag{8.16}$$

Figures 8.12 to 8.14 show the results for this configuration. σ_7 and σ_3 are greater than 0 for every position of the typical range of motion, so every position is stable and at least this range of motion is safe to operate in.

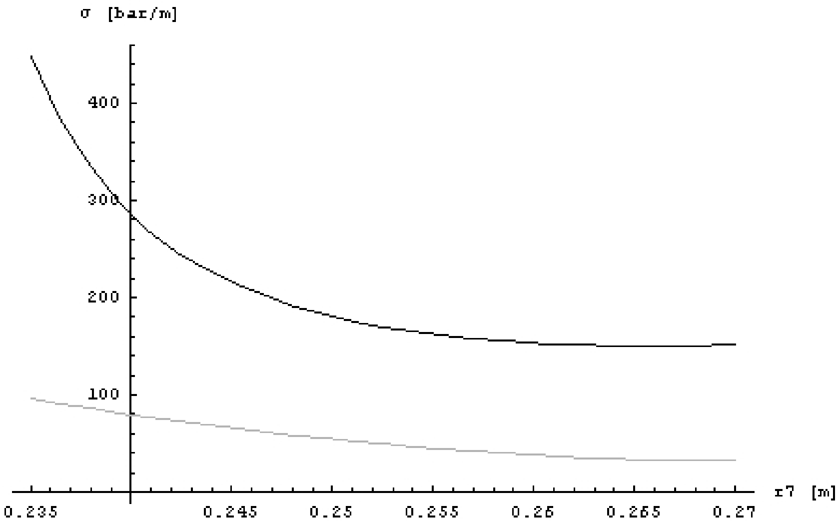

Figure 8.13: stability of cylinder r_7 (black) and cylinder r_3 (grey) when standing

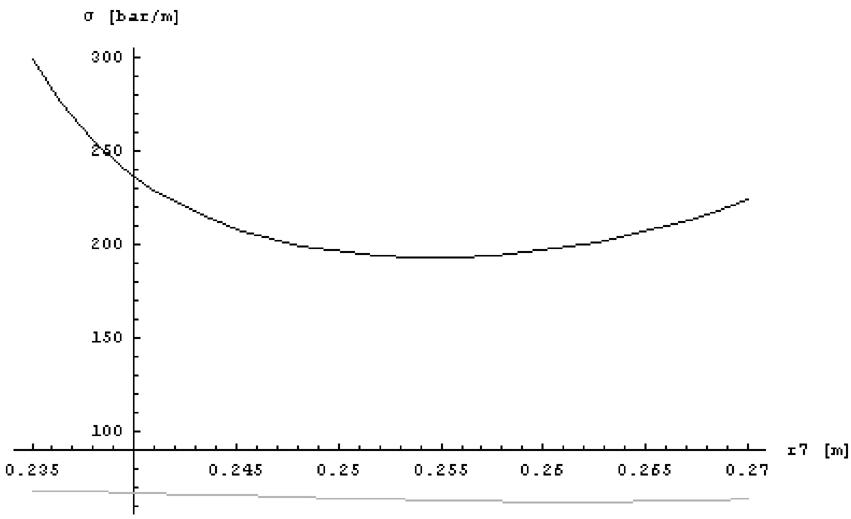

Figure 8.14: stability of cylinder r_7 (black) and cylinder r_3 (grey) when lifting a leg off the ground

The source code that is needed to create the plots can be found in appendix B.7. As r_3 is a function of r_7 for the typical range of motion, Δr_3 is calculated depending on Δr_7.

8.3.2 Whole range of motion

The stability could be mapped for the whole range of motion in a similar way in which it was developed for the typical range of motion. However there is no point in modelling the stability over the whole range as in practice some parts of the range of motion are inaccessible.

8.4 Dead points

Depending on the design some mechanism can lock. A point at which that happens is called a dead point. The four-bar linkage shown in figure 8.15 for example stalls in the dashed position if link 2 is driven (Mabie & Reinholtz 1987*b*).

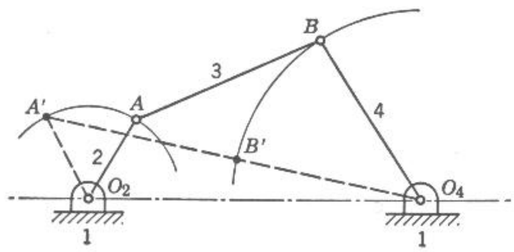

Figure 8.15: 4 bar linkage

The legs of Robug IV were originally designed in a way that prevents stalling in a position. The added spring mechanism does not change this as the kinematics of the leg remain unchanged. During the tests no configuration could be found that made the leg lock.

8.5 Summary

The further analysis of the spring mechanism shows that it will not only be possible to operate the Robug using the typical range of motion, but a more extended one is possible.

The leg with its spring mechanism is designed in a way that is stable and does not lock.

Chapter 9

Conclusions and Further Work

9.1 Achievement of Project Objectives

The following objectives have been addressed in this project:

Literature review of legged robotics

An investigation into legged robotics was carried out. Chapter 2 gives an overview of the history of legged robotics and introduces a number of legged robots that have been built.

Background and historical development of the Robug projects

The Robug that this project was based on is Robug IV, the fourth robot in a series of legged robotics projects. Chapter 3 introduces all 4 Robugs that have been built so far.

Design of an exoskeletal system to reduce the cylinder loads

A spring mechanism was developed that effectively reduces the cylinder loads. Chapter 4 deals with the development of the necessary model. In chapter 6 the design process is described.

Modelling the behaviour of this system on Robug

Chapter 4 describes the development of the model. It was used to investigate several aspects of the behaviour of the exoskeletal system. Chapter 8 describes the results. It will be possible to operate the Robug using a wide range of motion.

Manufacture and assembly of the exoskeletal system

Chapter 7 gives information about the manufacture of the spring mechanism. Due to an error within the model not enough time was left to manufacture the correct plates, but plates similar to these already existed and were assembled.

Test and quantification of the behaviour of the system

A test arrangement was used to run several tests. These are described and compared with the model in chapter 5. The model was found to be accurate for most cases. It was not possible to test the final system on the Robug itself, as the necessary software to operate the cylinders was not available at the completion date of this project.

9.2 Further Work

There are several more aspects of the new exoskeletal system that could not be addressed due to time constraints and due to the fact that a working control system and software for the Robug did not exist.

9.2.1 Test and quantification of the final system

To exactly quantify the behaviour of the new exoskeletal system it is necessary to test the system on the Robug itself. This could not be achieved as the necessary software to run such a test could not be completed before the completion date of this project. Tests were performed with a passive leg in a different environment as described in chapter 5, but these cannot completely replace a test on the Robug.

9.2.2 Other modes of operation

In this project the Robug was always assumed to be in a horizontal position. But what happens when the Robug climbs a hill or walks down stairs? This would have been another very interesting aspect to include in this project.

References

ASL (2005), *Robotics - Walking Machines*, Active Structure Laboratory, Free University of Brussels.
`http://www.ulb.ac.be/scmero/robotics.html#walking`
current October 2005.

Clippard Instrument Laboratory (2005*a*), *stainless steel cylinders: CDR-24-1*, Clippard Instrument Laboratory, Inc.
`http://www.clippard.com/store/display_details.asp?sku=CDR-24-1`
current October 2005.

Clippard Instrument Laboratory (2005*b*), *stainless steel cylinders: UDR-20-1*, Clippard Instrument Laboratory, Inc.
`http://www.clippard.com/store/display_details.asp?sku=UDR-20-1`
current October 2005.

Galt, S. (1998), *Soft Computing Based Motion Control for an Eight Legged Robot*, University of Portsmouth, Dept. of Electrical and Electronic Engineering, Portsmouth.

Honda (2001), *Asimo Timeline*, Honda Motor Co., Ltd.
`http://www.honda-robots.com/english/html/asimo/subframe5.html`
current October 2005.

Honda (2005), *History - Robot Development Process*, Honda Motor Co., Ltd.
`http://world.honda.com/ASIMO/history/`
current October 2005.

Lewis, M. A. (2002), 'Perception driven robot locomotion', *Journal Robot Society of Japan* **20**(3), 51–56.

Mabie, H. H. & Reinholtz, C. F. (1987*a*), *Mechanisms and dynamics of machinery*, 4th edn, John Wiley & Sons, New York, chapter 2.3, pp. 26–29.

Mabie, H. H. & Reinholtz, C. F. (1987*b*), *Mechanisms and dynamics of machinery*, 4th edn, John Wiley & Sons, New York, chapter 2.1, pp. 20+.

Malkamaki, B. (2004), *The Big Muskie - Remembering the walking giant*, Hi-Tech Design Internet Publishing.
`http://little-mountain.com/bigmuskie/`
current October 2005.

MECANT, the Walking Machine (2005), Automation Technology Laboratory, Helsinki University of Technology.
`http://www.automation.hut.fi/research/robotics/walking/mecant.htm`
current October 2005.

Milestones in the Development of Legged Robots (1999), MIT Leg Laboratory.
`http://www.ai.mit.edu/projects/leglab/background/milestones.html`
current October 2005.

Miller, A. & Hemsath, D. (2004), *Guide to the Eadweard Muybridge Collection*, University Archives and Records Center University of Pennsylvania.
`http://www.archives.upenn.edu/faids/upt/upt50/muybridgee.html`
current October 2005.

Robug III (2000), Nova Online.
`http://www.pbs.org/wgbh/nova/robots/hazard/meetrobug.html`
current October 2005.

Song, S.-M. & Waldron, K. J. (1988), *Machines That Walk: The Adaptive Suspension Vehicle*, The MIT Press, Cambridge, MA, USA.

Staunen, was die Zukunft bringt (2003), LpB Baden-Wuerttemberg.
`http://www.lpb.bwue.de/aktuell/puu/3_03/bau_b.htm`
current October 2005.

Waterman, R., Hewer, N. & Cooke, D. (n.d.), *Robug IV*.
`http://www.uwe.ac.uk/clawar/newsletters/issue3/RobugIV.html`
current October 2005.

Witte, H. (2000), *Biologische Inspiration des Baus einer vierbeinigen Laufmaschine - Anspruch und Wirklichkeit*, University of Duisburg.
`http://www.mechatronik.uni-duisburg.de/seminar/witte.html`
current October 2005.

Wolfram Research (2005*a*), *Mathematica Documentation: Findroot*, Wolfram Research, Inc.
`http://documents.wolfram.com/mathematica/functions/FindRoot`
current October 2005.

Wolfram Research (2005*b*), *Mathematica Documentation: LinearSolve*, Wolfram Research, Inc.
`http://documents.wolfram.com/mathematica/functions/LinearSolve`
current October 2005.

WorkPartner - Information (2005), Automation Technology Laboratory, Helsinki University of Technology.
`http://www.automation.hut.fi/IMSRI/workpartner/information.html`
current October 2005.

Appendix A

Project Specification

University of Southern Queensland
Faculty of Engineering and Surveying

ENG 4111/4112 Research Project
PROJECT SPECIFICATION

FOR: **Nils Lückemeyer**

TOPIC: Assisted standing and walking mode for RobugIV eight legged robot

SUPERVISORS: Chris Snook
Prof John Billingsley

PROJECT AIM: This project aims to provide a mechanical structure for the legs of RobugIV that allows it to stand up and be operated at lower air pressures.

SPONSORSHIP: Faculty of Engineering and Surveying

PROGRAMME: **Issue A; 15 June 2005**

1. Review the background and historical development of the Robug legged robot;
2. Conduct a literature review of legged robots;
3. Design an exoskeletal system to reduce the cylinder loads on Robug whilst standing;
4. Develop techniques to model the behaviour of this system on Robug;
5. Liaise with workshop staff in the manufacture and assembly of the exoskeletal system;
6. Test and quantify the behaviour of the system;

As time permits:

7. Investigate other modes of operation of Robug

AGREED:

________________ (Student) ________________, ________________ (Supervisors)

____/____/____ ____/____/____ ____/____/____

Figure A.1: Project Specification

Appendix B

Source Code

B.1 Introduction

This appendix consists of different source codes written in MATHEMATICA. The main code for the model can be found in section B.3. Most of the other programs use the model code as a subroutine.

The variables used are explained along with the source code.

B.2 Starting values

This is a little routine that calculates starting values for the angles ϕ_2, ϕ_3, ϕ_4, ϕ_5, ϕ_7 and ϕ_8. The values for $start_i$ are guesses.

Table B.1: nomenclature

expression	explanation
$start_i$	guessed starting values
r_i	lengths of links
$a_i,\ b_i$	partial lengths
ϕ_i	angles
$erg1$	result for the angles

```
start[2] = 2.5;
start[3] = 3;
start[4] = 2.5;
start[5] = 1.5;
start[7] = 0;
start[8] = 4.5;

r[7] = .2525;
r[3] = .3325;

r[1] = .104;
r[2] = .334;
r[4] = .098;
r[5] = .057;
r[6] = .066;
r[9] = .397;

a[3] = .057;
a[8] = .074;

b[3] = .007;

         22
ϕ[1] = ─── π;
        180
ϕ[6] = 1.867;


erg1 = FindRoot[{
   r[1] Sin[ϕ[1]] + r[4] Sin[ϕ[4]] - r[6] Sin[ϕ[5] + ϕ[6] - π] -
     r[5] Sin[ϕ[5]] - b[3] Sin[ϕ[3] - .5 π] - a[3] Sin[ϕ[3]] == 0,
   r[1] Cos[ϕ[1]] + r[4] Cos[ϕ[4]] - r[6] Cos[ϕ[5] + ϕ[6] - π] -
     r[5] Cos[ϕ[5]] - b[3] Cos[ϕ[3] - .5 π] - a[3] Cos[ϕ[3]] == 0,
   r[5] Sin[ϕ[5]] - r[7] Sin[ϕ[7]] + a[8] Sin[ϕ[8]] -
     (r[3] - a[3]) Sin[ϕ[3]] + b[3] Sin[ϕ[3] - .5 π] == 0,
   r[5] Cos[ϕ[5]] - r[7] Cos[ϕ[7]] + a[8] Cos[ϕ[8]] -
     (r[3] - a[3]) Cos[ϕ[3]] + b[3] Cos[ϕ[3] - .5 π] == 0,
   r[2] Sin[ϕ[2]] + a[8] Sin[ϕ[8]] - r[3] Sin[ϕ[3]] == 0,
   r[2] Cos[ϕ[2]] + a[8] Cos[ϕ[8]] - r[3] Cos[ϕ[3]] == 0
  }, {{ϕ[2], start[2]}, {ϕ[3], start[3]}, {ϕ[4], start[4]},
   {ϕ[5], start[5]}, {ϕ[7], start[7]}, {ϕ[8], start[8]}}]

{ϕ[2] → 2.54484, ϕ[3] → 2.76731, ϕ[4] → 2.49031,
 ϕ[5] → 1.49132, ϕ[7] → -0.422426, ϕ[8] → 4.24702}
```

Figure B.1: source code to calculate the starting values

B.3 Model

This is the main code of the model. It defines a routine p in which all the kinematics and kinetics are calculated. It also includes the option to create a sketch of the leg at the position that is evaluated.

```
<< Graphics`MultipleListPlot`

start[2] = 2.545;
start[3] = 2.767;
start[4] = 2.490;
start[5] = 1.491;
start[7] = -0.4224;
start[8] = 4.247;

p[cupper_, clower_, n_, h_, f1_, f2_] := Module[{φ, erg1, b},

   r[7] = cupper;
   r[3] = clower;

   r[1] = .104;
   r[2] = .334;
   r[4] = .098;
   r[5] = .057;
   r[6] = .066;
   r[9] = .397;

   a[3] = .057;
   a[8] = .074;

   b[3] = .007;

   φ[1] = 22/180 π;
   φ[6] = 1.867;


   erg1 = FindRoot[{
      r[1] Sin[φ[1]] + r[4] Sin[φ[4]] - r[6] Sin[φ[5] + φ[6] - π] -
        r[5] Sin[φ[5]] - b[3] Sin[φ[3] - .5 π] - a[3] Sin[φ[3]] == 0,
      r[1] Cos[φ[1]] + r[4] Cos[φ[4]] - r[6] Cos[φ[5] + φ[6] - π] -
        r[5] Cos[φ[5]] - b[3] Cos[φ[3] - .5 π] - a[3] Cos[φ[3]] == 0,
      r[5] Sin[φ[5]] - r[7] Sin[φ[7]] + a[8] Sin[φ[8]] -
        (r[3] - a[3]) Sin[φ[3]] + b[3] Sin[φ[3] - .5 π] == 0,
      r[5] Cos[φ[5]] - r[7] Cos[φ[7]] + a[8] Cos[φ[8]] -
        (r[3] - a[3]) Cos[φ[3]] + b[3] Cos[φ[3] - .5 π] == 0,
      r[2] Sin[φ[2]] + a[8] Sin[φ[8]] - r[3] Sin[φ[3]] == 0,
      r[2] Cos[φ[2]] + a[8] Cos[φ[8]] - r[3] Cos[φ[3]] == 0
     }, {{φ[2], start[2]}, {φ[3], start[3]}, {φ[4], start[4]},
      {φ[5], start[5]}, {φ[7], start[7]}, {φ[8], start[8]}}, AccuracyGoal → 4];

   φ[2] = φ[2] /. erg1;
   φ[3] = φ[3] /. erg1;
   φ[4] = φ[4] /. erg1;
   φ[5] = φ[5] /. erg1;
   φ[7] = φ[7] /. erg1;
   φ[8] = φ[8] /. erg1;

   φ[9] = φ[8] - 19/180 π;
```

Figure B.2: model source code page 1

```
punkt[0] = {0, 0};
punkt[1] = {r[1] Cos[φ[1]], r[1] Sin[φ[1]]};
punkt[2] = {r[2] Cos[φ[2]], r[2] Sin[φ[2]]};
punkt[3] = {r[3] Cos[φ[3]], r[3] Sin[φ[3]]};
punkt[4] = {r[1] Cos[φ[1]] + r[4] Cos[φ[4]], r[1] Sin[φ[1]] + r[4] Sin[φ[4]]};
punkt[5] =
 {a[3] Cos[φ[3]] + b[3] Cos[φ[3] - .5 π], a[3] Sin[φ[3]] + b[3] Sin[φ[3] - .5 π]};
punkt[6] = {r[2] Cos[φ[2]] + r[7] Cos[φ[7]], r[2] Sin[φ[2]] + r[7] Sin[φ[7]]};
punkt[7] = {a[3] Cos[φ[3]], a[3] Sin[φ[3]]};
punkt[8] = {r[3] Cos[φ[3]] + r[9] Cos[φ[9]], r[3] Sin[φ[3]] + r[9] Sin[φ[9]]};
punkt[9] = {r[1] Cos[φ[1]] + r[4] Cos[φ[4]] + h Cos[φ[4] - .5 π],
  r[1] Sin[φ[1]] + r[4] Sin[φ[4]] + h Sin[φ[4] - .5 π]};
punkt[10] = {r[1] Cos[φ[1]] + h Cos[φ[4] - .5 π], r[1] Sin[φ[1]] + h Sin[φ[4] - .5 π]};
punkt[11] = {r[1] Cos[φ[1]] + (r[4] - n) Cos[φ[4]] + h Cos[φ[4] - .5 π],
  r[1] Sin[φ[1]] + (r[4] - n) Sin[φ[4]] + h Sin[φ[4] - .5 π]};

list1 = {punkt[4], punkt[1], punkt[10],
  punkt[9], punkt[4], punkt[6], punkt[5], punkt[7]};
list2 = {punkt[8], punkt[3], punkt[2], punkt[6]};
list3 = {punkt[3], punkt[0], punkt[2]};
list4 = {punkt[0], punkt[11]};

If [grafik == 1, MultipleListPlot[list1, list2, list3, list4, Axes → False,
  PlotRange → {{-.8, .3}, {-.6, .6}}, SymbolShape → None, PlotJoined → True,
  PlotStyle → {GrayLevel[0], GrayLevel[0], GrayLevel[0], RGBColor[0, 0, 1]},
  AspectRatio → Automatic],];

r[10] = 0.00875 + Sqrt[punkt[11]⟦1⟧^2 + punkt[11]⟦2⟧^2];
φ[10] = ArcTan[punkt[11]⟦1⟧, punkt[11]⟦2⟧];

l[1] = .165;
l[2] = .090;
l[3] = .150;
l[5] = .035;
l[6] = .065;
height[1] = .03;

g[1] = 9.81 * .6;
g[2] = 9.81 * 1.35;
g[3] = 9.81 * 1.2;
g[4] = 9.81 * .2;
g[5] = 9.81 * .05;
g[6] = 9.81 * .1;

s = 6434 (r[10] - 0.10115);

mat = {{1, 0, 0, 1, 1, 0, 0, 0, 0, 0, 0, 0, 0, 0, 0},
  {0, 1, 1, 0, 0, 1, 0, 0, 0, 0, 0, 0, 0, 0, 0}, {Cos[φ[9]] r[9], -r[9] Sin[φ[9]],
   0, 0, -a[8] Cos[φ[8]], a[8] Sin[φ[8]], 0, 0, 0, 0, 0, 0, 0, 0, 0}, {0, 0, 0, 0,
   0, 0, 0, 0, 0, -1, 0, 0, 1, 1, 0}, {0, 0, 0, 0, 0, 0, 0, 0, 0, 0, -1, 1, 0, 0, 1},
  {0, 0, 0, 0, 0, 0, 0, 0, 0, 0, 0, r[6] Sin[φ[5] + φ[6]], -Cos[φ[5] + φ[6]] r[6],
   -Cos[φ[5]] r[5], r[5] Sin[φ[5]]}, {0, 0, 0, 0, 0, 0, 0, 0, -1, 0, 1, 0, 0, 0, 0},
  {0, 0, 0, 0, 0, 0, 0, -1, 0, 1, 0, 0, 0, 0, 0},
  {0, 0, 0, 0, 0, 0, 0, Cos[φ[7]] r[7], -r[7] Sin[φ[7]], 0, 0, 0, 0, 0, 0},
```

Figure B.3: model source code page 2

```
  {0, 0, r[3] Sin[ϕ[3]], -Cos[ϕ[3]] r[3], 0, 0, 0, 0, 0, 0, 0, 0, 0,
   -a[3] Cos[ϕ[3]] - b[3] Sin[ϕ[3]], a[3] Sin[ϕ[3]] - b[3] Cos[ϕ[3]]},
  {0, 0, 0, 0, 0, -1, Cos[ϕ[2]], 0, 1, 0, 0, 0, 0, 0, 0},
  {0, 0, 0, 0, -1, 0, Sin[ϕ[2]], 1, 0, 0, 0, 0, 0, 0, 0},
  {0, 0, 0, 0, 0, 0, 0, 0, 0, 0, 0, r[4] Sin[ϕ[4]], -Cos[ϕ[4]] r[4], 0, 0},
  {1, 0, 0, 0, 0, 0, 0, 0, 0, 0, 0, 0, 0, 0, 0},
  {0, 1, 0, 0, 0, 0, 0, 0, 0, 0, 0, 0, 0, 0, 0}};

b = {g[1] + g[4], 0, g[1] (l[1] Cos[ϕ[9]] + height[1] Cos[ϕ[9] - .5 π]), 0,
  0, 0, 0, g[2] + g[5], -g[2] l[2] Cos[ϕ[7]] - g[5] (r[7] - l[5]) Cos[ϕ[7]],
  -g[3] l[3] Cos[ϕ[3] - π] - g[6] (r[3] - l[6]) Cos[ϕ[3] - π],
  0, 0, -s * r[1] Sin[ϕ[10] - ϕ[1]], f1, f2};

kraft = LinearSolve[mat, b];

z3 = 0.0129 (kraft[[4]] Sin[ϕ[3] - π] + kraft[[3]] Cos[ϕ[3] - π] + g[6] Sin[ϕ[3] - π]);
z7 = 0.00912 (kraft[[8]] Sin[ϕ[7]] + kraft[[9]] Cos[ϕ[7]] + g[5] Sin[ϕ[7]]);


];
```

Figure B.4: model source code page 3

Table B.2: Nomenclature for the model. Protected expressions can only be seen within the model they are used in.

expressions	explanation
$start_i$	calculated starting values
p	module that calculates the mechanics
$n,\ h$	position of the spring on the plates
$F_1,\ F_2$	forces on the foot
r_7	lengths of the upper cylinder
r_3	lengths of the lower cylinder
r_i	lengths of links
$a_i,\ b_i$	partial lengths
ϕ_i	angles (protected)
$erg1$	result for the angles (protected)
$punkt_i$	coordinates of end points of links
$list_i$	lists of end points to make a sketch
$l_i,\ height_1$	lengths to describe the positions of weights
g_i	weights
s	equivalent spring force
mat	matrix for the force equations
b	vector (right side of the force equations, protected)
$kraft$	force vector (contains F_1 to F_{15})
z_i	cylinder pressures
$grafik$	plot / do not plot a sketch of the leg

B.4 Model Validation

B.4.1 Modified model

A few modifications had to be made to make the test arrangement and the model comparable. The module that calculates the modified mechanics is called $modified(r_7, r_3, n)$, where n describes the spring position, $n = 1, 2, ..., 8$.

```
<< Graphics`MultipleListPlot`

start[2] = 2.545;
start[3] = 2.767;
start[4] = 2.490;
start[5] = 1.491;
start[7] = -0.4224;
start[8] = 4.247;

modified[cupper_, clower_, n_] := Module[{φ, erg1, b},

  r[7] = cupper;
  r[3] = clower;

  r[1] = .104;
  r[2] = .334;
  r[4] = .098;
  r[5] = .057;
  r[6] = .066;
  r[9] = .397;

  a[3] = .057;
  a[8] = .074;

  b[3] = .007;

  h = .057;

          22
  φ[1] = ─── π;
         180
  φ[6] = 1.867;


  erg1 = FindRoot[{
     r[1] Sin[φ[1]] + r[4] Sin[φ[4]] - r[6] Sin[φ[5] + φ[6] - π] -
       r[5] Sin[φ[5]] - b[3] Sin[φ[3] - .5 π] - a[3] Sin[φ[3]] == 0,
     r[1] Cos[φ[1]] + r[4] Cos[φ[4]] - r[6] Cos[φ[5] + φ[6] - π] -
       r[5] Cos[φ[5]] - b[3] Cos[φ[3] - .5 π] - a[3] Cos[φ[3]] == 0,
     r[5] Sin[φ[5]] - r[7] Sin[φ[7]] + a[8] Sin[φ[8]] -
       (r[3] - a[3]) Sin[φ[3]] + b[3] Sin[φ[3] - .5 π] == 0,
     r[5] Cos[φ[5]] - r[7] Cos[φ[7]] + a[8] Cos[φ[8]] -
       (r[3] - a[3]) Cos[φ[3]] + b[3] Cos[φ[3] - .5 π] == 0,
     r[2] Sin[φ[2]] + a[8] Sin[φ[8]] - r[3] Sin[φ[3]] == 0,
     r[2] Cos[φ[2]] + a[8] Cos[φ[8]] - r[3] Cos[φ[3]] == 0
    }, {{φ[2], start[2]}, {φ[3], start[3]}, {φ[4], start[4]},
     {φ[5], start[5]}, {φ[7], start[7]}, {φ[8], start[8]}}];

  φ[2] = φ[2] /. erg1;
  φ[3] = φ[3] /. erg1;
  φ[4] = φ[4] /. erg1;
  φ[5] = φ[5] /. erg1;
  φ[7] = φ[7] /. erg1;
  φ[8] = φ[8] /. erg1;
```

Figure B.5: modified model source code page 1

```
ϕ[9] = ϕ[8] - 19/180 π;

punkt[0] = {0, 0};
punkt[1] = {r[1] Cos[ϕ[1]], r[1] Sin[ϕ[1]]};
punkt[2] = {r[2] Cos[ϕ[2]], r[2] Sin[ϕ[2]]};
punkt[3] = {r[3] Cos[ϕ[3]], r[3] Sin[ϕ[3]]};
punkt[4] = {r[1] Cos[ϕ[1]] + r[4] Cos[ϕ[4]], r[1] Sin[ϕ[1]] + r[4] Sin[ϕ[4]]};
punkt[5] =
 {a[3] Cos[ϕ[3]] + b[3] Cos[ϕ[3] - .5 π], a[3] Sin[ϕ[3]] + b[3] Sin[ϕ[3] - .5 π]};
punkt[6] = {r[2] Cos[ϕ[2]] + r[7] Cos[ϕ[7]], r[2] Sin[ϕ[2]] + r[7] Sin[ϕ[7]]};
punkt[7] = {a[3] Cos[ϕ[3]], a[3] Sin[ϕ[3]]};
punkt[8] = {r[3] Cos[ϕ[3]] + r[9] Cos[ϕ[9]], r[3] Sin[ϕ[3]] + r[9] Sin[ϕ[9]]};
punkt[9] = {r[1] Cos[ϕ[1]] + r[4] Cos[ϕ[4]] + h Cos[ϕ[4] - .5 π],
  r[1] Sin[ϕ[1]] + r[4] Sin[ϕ[4]] + h Sin[ϕ[4] - .5 π]};
punkt[10] = {r[1] Cos[ϕ[1]] + h Cos[ϕ[4] - .5 π], r[1] Sin[ϕ[1]] + h Sin[ϕ[4] - .5 π]};
punkt[11] = {r[1] Cos[ϕ[1]] + (8/7 - n/7) r[4] Cos[ϕ[4]] + h Cos[ϕ[4] - .5 π],
  r[1] Sin[ϕ[1]] + (8/7 - n/7) r[4] Sin[ϕ[4]] + h Sin[ϕ[4] - .5 π]};

list1 = {punkt[4], punkt[1], punkt[10],
  punkt[9], punkt[4], punkt[6], punkt[5], punkt[7]};
list2 = {punkt[8], punkt[3], punkt[2], punkt[6]};
list3 = {punkt[3], punkt[0], punkt[2]};
list4 = {punkt[0], punkt[11]};

grafik = 0;
If [grafik == 1, MultipleListPlot[list1, list2, list3, list4, Axes → False,
  PlotRange → {{-.8, .15}, {-.6, .35}}, SymbolShape → None, PlotJoined → True,
  PlotStyle → {GrayLevel[0], GrayLevel[0], GrayLevel[0], RGBColor[0, 0, 1]},
  AspectRatio → Automatic],];

r[10] = 0.00875 + Sqrt[punkt[11][[1]]^2 + punkt[11][[2]]^2];
ϕ[10] = ArcTan[punkt[11][[1]], punkt[11][[2]]];

l[1] = .165;
l[2] = .090;
l[3] = .150;
l[5] = .035;
l[6] = .065;
height[1] = .03;

g[1] = -9.81 * .6;
g[2] = -9.81 * 1.35;
g[3] = -9.81 * 1.2;
g[4] = -9.81 * .2;
g[5] = -9.81 * .05;
g[6] = -9.81 * .1;

s = 6434 (r[10] - 0.10115);

mat = {{1, 0, 0, 1, 1, 0, 0, 0, 0, 0, 0, 0, 0, 0, 0},
  {0, 1, 1, 0, 0, 1, 0, 0, 0, 0, 0, 0, 0, 0, 0}, {Cos[ϕ[9]] r[9], -r[9] Sin[ϕ[9]],
   0, 0, -a[8] Cos[ϕ[8]], a[8] Sin[ϕ[8]], 0, 0, 0, 0, 0, 0, 0, 0, 0}, {0, 0, 0, 0,
```

Figure B.6: modified model source code page 2

```
  0, 0, 0, 0, 0, -1, 0, 0, 1, 1, 0}, {0, 0, 0, 0, 0, 0, 0, 0, 0, 0, -1, 1, 0, 0, 1},
 {0, 0, 0, 0, 0, 0, 0, 0, 0, 0, 0, r[6] Sin[ϕ[5] + ϕ[6]], -Cos[ϕ[5] + ϕ[6]] r[6],
  -Cos[ϕ[5]] r[5], r[5] Sin[ϕ[5]]}, {0, 0, 0, 0, 0, 0, 0, 0, -1, 0, 1, 0, 0, 0, 0},
 {0, 0, 0, 0, 0, 0, 0, -1, 0, 1, 0, 0, 0, 0, 0},
 {0, 0, 0, 0, 0, 0, 0, Cos[ϕ[7]] r[7], -r[7] Sin[ϕ[7]], 0, 0, 0, 0, 0, 0},
 {0, 0, r[3] Sin[ϕ[3]], -Cos[ϕ[3]] r[3], 0, 0, 0, 0, 0, 0, 0, 0, 0,
  -a[3] Cos[ϕ[3]] - b[3] Sin[ϕ[3]], a[3] Sin[ϕ[3]] - b[3] Cos[ϕ[3]]},
 {0, 0, 0, 0, 0, -1, Cos[ϕ[2]], 0, 1, 0, 0, 0, 0, 0, 0},
 {0, 0, 0, 0, -1, 0, Sin[ϕ[2]], 1, 0, 0, 0, 0, 0, 0, 0},
 {0, 0, 0, 0, 0, 0, 0, 0, 0, 0, 0, r[4] Sin[ϕ[4]], -Cos[ϕ[4]] r[4], 0, 0},
 {0, 0, 0, 0, 0, 0, 0, Sin[ϕ[7]], Cos[ϕ[7]], 0, 0, 0, 0, 0, 0},
 {0, 1, 0, 0, 0, 0, 0, 0, 0, 0, 0, 0, 0, 0, 0}};

b = {g[1] + g[4], 0, g[1] (l[1] Cos[ϕ[9]] + height[1] Cos[ϕ[9] - .5 π]), 0,
  0, 0, 0, g[2] + g[5], -g[2] l[2] Cos[ϕ[7]] - g[5] (r[7] - l[5]) Cos[ϕ[7]],
  -g[3] l[3] Cos[ϕ[3] - π] - g[6] (r[3] - l[6]) Cos[ϕ[3] - π],
  0, 0, -s * r[1] Sin[ϕ[10] - ϕ[1]], -g[5] Sin[ϕ[7]], 0};

kraft = LinearSolve[mat, b];


];
```

Figure B.7: modified model source code page 3

B.4.2 Comparison of model and test

Figure B.8 shows the source code that creates one of the plots which compares the model with the test arrangement results. All comparison plots use a similar source code.

Table B.3: Additional nomenclature for the comparison plots.

expressions	explanation
$versuch$	list of all test arrangement data
$vers$	list of selected test arrangement data
$modell$	list of corresponding model data

```
versuch = {{.229, .291, 1, 3.9}, {.231, .291, 1, 3.6}, {.235, .291, 1, 3.4},
   {.241, .291, 1, 3.2}, {.259, .291, 1, 2.7}, {.273, .291, 1, 2.2},

   {.228, .287, 3, 2.4}, {.231, .287, 3, 2.2}, {.253, .287, 3, 1.9},
   {.272, .287, 3, 1.2}, {.278, .287, 3, 0.9}, {.288, .287, 3, 0},

   {.227, .287, 5, 1}, {.265, .287, 5, .9}, {.281, .287, 5, .7}, {.289, .287, 5, 0},

   {.286, .336, 1, 0}, {.275, .336, 1, .6},
   {.270, .336, 1, .9}, {.264, .336, 1, 1.2}, {.253, .336, 1, 1.5},
   {.246, .336, 1, 1.8}, {.237, .336, 1, 2.2}, {.229, .336, 1, 2.6},

   {.285, .381, 1, 0}, {.277, .381, 1, .4}, {.265, .381, 1, .8},
   {.256, .381, 1, 1.2}, {.246, .381, 1, 1.6}, {.239, .381, 1, 2},

   {.280, .336, 3, 0}, {.265, .336, 3, .6},
   {.253, .336, 3, .9}, {.241, .336, 3, 1.2}, {.228, .336, 3, 1.5},

   {.275, .336, 5, 0}, {.259, .336, 5, 0.2}, {.249, .336, 5, 0.4}, {.238, .336, 5, 0.5},

   {.267, .381, 5, 0}, {.255, .381, 5, 0.2}, {.238, .381, 5, 0.4},

   {.273, .381, 4, 0}, {.264, .381, 4, 0.2},
   {.254, .381, 4, 0.4}, {.245, .381, 4, 0.6}, {.237, .381, 4, 0.9}

  };
vers = Table[{versuch[[i, 1]], versuch[[i, 4]] * 9.81}, {i, 31, 35}];
modell = Table[{i, modified[i, .336, 3]; kraft[[1]]}, {i, .225, .290, .001}];
MultipleListPlot[vers, modell, PlotRange → {{.22, .290}, {-10, 40}},
 SymbolShape → {PlotSymbol[Box], None}, PlotJoined → {False, True},
 PlotStyle → {GrayLevel[0], RGBColor[0, 0, 1]},
 PlotLabel -> "Comparison of model and experiment",
 AxesLabel → {"upp. cyl. [m]", "foot force [N]"}]
```

Figure B.8: comparison of model and test source code

B.5 Mechanism design

This code first defines a module $maxp(n, h)$ which gives the maximum pressures of the typical range of motion for a given spring position. This module is then used to plot figures 6.1 and 6.2.

```
maxp[n_, h_] := Module[{},

   grafik = 0;
   zylmax = 0;
   zylnummer = 0;
   zyl7pos = 0;

   Do[
    p[i, 14.071 i^2 - 6.345 i + 1.028, n, h, 63.52, 0];
    If[Abs[z7] > Abs[zylmax],
     zylmax = z7; zyl7pos = i; zylnummer = 7; art = "stand up"];
    If[Abs[z3] > Abs[zylmax], zylmax = z3; zyl7pos = i;
     zylnummer = 3; art = "stand up"],
    {i, .235, .270, .002}];

   p[.265, .3347, n, h, 84.7, 0];
   If[Abs[z7] > Abs[zylmax],
    zylmax = z7; zyl7pos = .260; zylnummer = 7; art = "stand"];
   If[Abs[z3] > Abs[zylmax], zylmax = z3; zyl7pos = .260; zylnummer = 3; art = "stand"];

   Do[
    p[i, 14.071 i^2 - 6.345 i + 1.028, n, h, 0, 0];
    If[Abs[z7] > Abs[zylmax],
     zylmax = z7; zyl7pos = i; zylnummer = 7; art = "lift leg"];
    If[Abs[z3] > Abs[zylmax], zylmax = z3; zyl7pos = i;
     zylnummer = 3; art = "lift leg"],
    {i, .250, .265, .002}];


   zylmax

  ];

ContourPlot[Abs[maxp[n, h]], {n, -.03, .07},
  {h, 0.02, 0.11}, AxesLabel → {"n [m]", "h [m]"}];
Plot[Abs[maxp[1.53 h - 0.0908, h]], {h, .020, .110},
 AxesLabel → {"h [m]", "maxp [bar]"}]
```

Figure B.9: maximum pressure source code

Table B.4: Additional nomenclature for the max. pressure source code.

expressions	explanation
$maxp(n, h)$	module that calculates the maximum pressure
zylmax	maximum pressure
zylnummer	cylinder in which *zylmax* occurs
zyl7pos	position at which *zylmax* occurs
art	type of motion during which *zylmax* occurs

B.6 Pressure plots

B.6.1 Typical range of motion

typical range pressure plots.nb 1

```
grafik = 0;
Plot[{p[i, 14.071 i^2 - 6.345 i + 1.028, 0.001, 0.060, 63.52, 0]; z7,
   p[i, 14.071 i^2 - 6.345 i + 1.028, 0.001, 0.060, 63.52, 0]; z3, 5, -5},
  {i, .235, .270}, AxesLabel → {"r7 [m]", "p [bar]"},
  PlotStyle → {GrayLevel[0], GrayLevel[0.5], GrayLevel[0.7], GrayLevel[0.7]}];
Plot[{p[i, 14.071 i^2 - 6.345 i + 1.028, 0.001, 0.060, 84.7, 0]; z7,
   p[i, 14.071 i^2 - 6.345 i + 1.028, 0.001, 0.060, 84.7, 0]; z3, 5, -5},
  {i, .235, .270}, AxesLabel → {"r7 [m]", "p [bar]"},
  PlotStyle → {GrayLevel[0], GrayLevel[0.5], GrayLevel[0.7], GrayLevel[0.7]}];
Plot[{p[i, 14.071 i^2 - 6.345 i + 1.028, 0.001, 0.060, 0, 0]; z7,
  p[i, 14.071 i^2 - 6.345 i + 1.028, 0.001, 0.060, 0, 0]; z3, 5, -5},
 {i, .235, .270}, AxesLabel → {"r7 [m]", "p [bar]"},
 PlotStyle → {GrayLevel[0], GrayLevel[0.5], GrayLevel[0.7], GrayLevel[0.7]}]
```

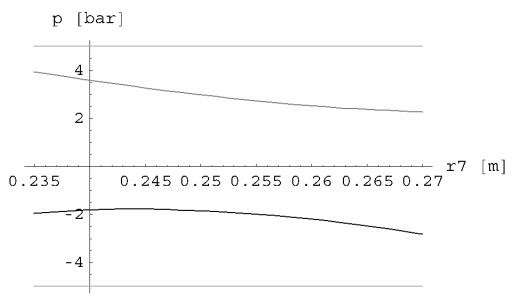

Figure B.10: source code used to plot the pressures for the typical range of motion

B.6.2 Whole range of motion

Code similar to the one shown in figure B.11 was used to plot the pressures in both cylinders for all three types of motion.

pressure plot.nb 1

```
grafik = 0;
Plot3D[p[i, j, 0.001, 0.060, 63.52, 0]; z7,
  {i, .225, .290}, {j, .285, .380},
  AxesLabel → {"r7 [m]", "r3 [m]", "p [bar]"}, ColorFunction → Hue];
MatrixForm[Table[p[i, j, 0.001, 0.060, 63.52, 0]; z7,
  {i, .225, .290, .003}, {j, .285, .380, .003}]]
```

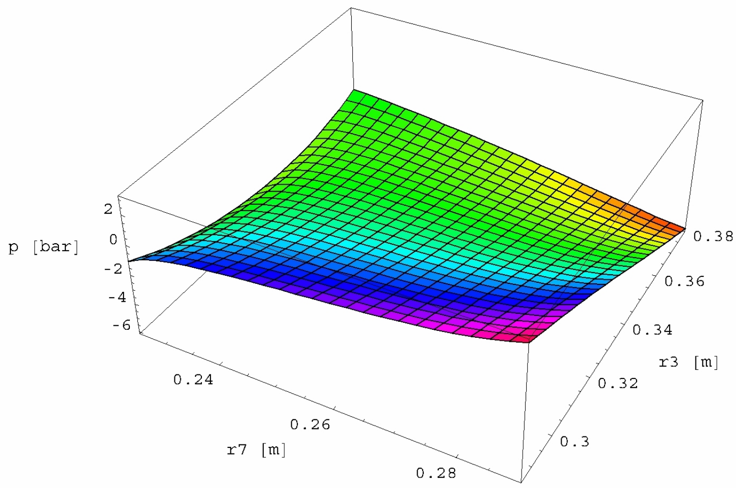

Figure B.11: source code used to plot the pressures for the whole range of motion

B.7 Stability

```
Plot[
  {({p[i, 14.071 i^2 - 6.345 i + 1.028, 0.001, 0.060, 63.52, 0]; pres = z7} -
      {j = i + 0.0001; p[j, 14.071 i^2 - 6.345 i + 1.028, 0.001, 0.060, 63.52, 0]; z7}) /
     0.0001 + If[pres > 0, (pres + 1) / (.300 - i) + 1 / (i - .225),
     (pres - 1) / (.225 - i) + 1 / (.300 - i)],
   ({p[i, 14.071 i^2 - 6.345 i + 1.028, 0.001, 0.060, 63.52, 0]; pres = z3} -
      {j = i + 0.0001; p[i, 14.071 j^2 - 6.345 j + 1.028, 0.001, 0.060, 63.52, 0]; z3}) /
     (14.071 j^2 - 6.345 j + 1.028 - (14.071 i^2 - 6.345 i + 1.028)) +
    If[pres > 0, (pres + 1) / (.380 - (14.071 i^2 - 6.345 i + 1.028)) +
      1 / ((14.071 i^2 - 6.345 i + 1.028) - .285), (pres - 1) /
       (.285 - (14.071 i^2 - 6.345 i + 1.028)) + 1 / (.380 - (14.071 i^2 - 6.345 i + 1.028))]},
  {i, .235, .270}, AxesLabel → {"r7 [m]", "σ [bar/m]"},
  PlotStyle → {GrayLevel[0], GrayLevel[.7]}];

Plot[
  {({p[i, 14.071 i^2 - 6.345 i + 1.028, 0.001, 0.060, 84.7, 0]; pres = z7} -
      {j = i + 0.0001; p[j, 14.071 i^2 - 6.345 i + 1.028, 0.001, 0.060, 84.7, 0]; z7}) /
     0.0001 + If[pres > 0, (pres + 1) / (.300 - i) + 1 / (i - .225),
     (pres - 1) / (.225 - i) + 1 / (.300 - i)],
   ({p[i, 14.071 i^2 - 6.345 i + 1.028, 0.001, 0.060, 84.7, 0]; pres = z3} -
      {j = i + 0.0001; p[i, 14.071 j^2 - 6.345 j + 1.028, 0.001, 0.060, 84.7, 0]; z3}) /
     (14.071 j^2 - 6.345 j + 1.028 - (14.071 i^2 - 6.345 i + 1.028)) +
    If[pres > 0, (pres + 1) / (.380 - (14.071 i^2 - 6.345 i + 1.028)) +
      1 / ((14.071 i^2 - 6.345 i + 1.028) - .285), (pres - 1) /
       (.285 - (14.071 i^2 - 6.345 i + 1.028)) + 1 / (.380 - (14.071 i^2 - 6.345 i + 1.028))]},
  {i, .235, .270}, AxesLabel → {"r7 [m]", "σ [bar/m]"},
  PlotStyle → {GrayLevel[0], GrayLevel[.7]}];

Plot[
 {({p[i, 14.071 i^2 - 6.345 i + 1.028, 0.001, 0.060, 0, 0]; pres = z7} -
     {j = i + 0.0001; p[j, 14.071 i^2 - 6.345 i + 1.028, 0.001, 0.060, 0, 0]; z7}) / 0.0001 +
   If[pres > 0, (pres + 1) / (.300 - i) + 1 / (i - .225),
    (pres - 1) / (.225 - i) + 1 / (.300 - i)],
  ({p[i, 14.071 i^2 - 6.345 i + 1.028, 0.001, 0.060, 0, 0]; pres = z3} -
     {j = i + 0.0001; p[i, 14.071 j^2 - 6.345 j + 1.028, 0.001, 0.060, 0, 0]; z3}) /
    (14.071 j^2 - 6.345 j + 1.028 - (14.071 i^2 - 6.345 i + 1.028)) +
   If[pres > 0, (pres + 1) / (.380 - (14.071 i^2 - 6.345 i + 1.028)) +
     1 / ((14.071 i^2 - 6.345 i + 1.028) - .285), (pres - 1) /
      (.285 - (14.071 i^2 - 6.345 i + 1.028)) + 1 / (.380 - (14.071 i^2 - 6.345 i + 1.028))]},
 {i, .235, .270}, AxesLabel → {"r7 [m]", "σ [bar/m]"},
 PlotStyle → {GrayLevel[0], GrayLevel[.7]}]
```

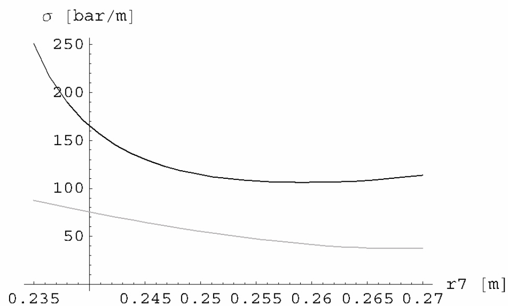

Figure B.12: source code used to examine the stability of a position within the typical range of motion